C.P. No. 410
(20,397)
A.R.C. Technical Report

C.P. No. 410
(20,397)
A.R.C. Technical Report

MINISTRY OF SUPPLY

AERONAUTICAL RESEARCH COUNCIL

CURRENT PAPERS

Low-speed Wind-tunnel Tests of the effects of Various Leading-edge Modifications on the Sectional Characteristics of a Thin Wing

by

S. F. J. Butler, M.Sc.

LONDON: HER MAJESTY'S STATIONERY OFFICE

1958

PRICE 7s. 6d. NET

C.P. No.410

U.D.C. No. 533.6.011.34: 533.692.1: 533.694.25

Technical Note No. Aero 2570

June, 1958

ROYAL AIRCRAFT ESTABLISHMENT

LOW-SPEED WIND-TUNNEL TESTS OF THE EFFECTS OF VARIOUS LEADING-EDGE MODIFICATIONS ON THE SECTIONAL CHARACTERISTICS OF A THIN WING (6% THICK, R.A.E. 101 SECTION)

by

S.F.J. Butler, M.Sc.

SUMMARY

The effects of various leading-edge modifications on the low-speed characteristics of a 6% thick R.A.E.101 aerofoil are discussed, with particular attention to the effects on the upper surface flow separations. In addition to the tests on the basic round-nosed section, the effects of attaching an isolated strake and a row of strakes to the leading edge were investigated. Tests were also made on a sharp-nosed version, both with and without deflected nose flap.

The results show that all the leading-edge modifications had profound effects on the upper surface flow separations. At the test Reynolds number (2×10^6), the upper surface of the basic round-nosed section exhibited a "short bubble" flow up to 5° incidence, above which incidence a "long bubble" developed, which spread to the wing trailing edge by 10°. Addition of a row of strakes inhibited the bubble growth and allowed a certain degree of peak negative pressure to occur near the leading edge, but the particular configuration tested did not increase CL_{max} or reduce the overall drag coefficient at a given lift coefficient. Addition of a sharp leading-edge extension caused the "long bubble" flow to develop from immediately above zero incidence. Deflection of the sharp leading edge caused the upper surface flow to remain attached, except for a localised region on the deflected nose, right up to the stall.

As a result of the changes in upper surface flow which were caused by the various leading-edge modifications, the chordwise pressure distributions and force and moment characteristics were also altered considerably.

A comparison is included between the measured pressure distributions, and distributions calculated assuming no flow separations to be present. This comparison demonstrates the desirability of employing a calculation method, such as that suggested in Refs.3,8 and 9, which allows for the effects of the "long bubble" separation.

LIST OF CONTENTS

LIST OF TABLES

LIST OF CONTENTS (Contd.)

LIST OF ILLUSTRATIONS

1 INTRODUCTION

This note describes the results of brief preliminary tests, made in the course of pressure-plotting investigations on a 6% thick R.A.E.101 aerofoil[1], to show the principal effects of various leading-edge modifications on the sectional characteristics of a thin wing, with particular attention to the effects on the upper surface flow separations.

In addition to the tests with the basic round-nosed symmetrical section, tests were made with a sharp leading-edge extension, with a deflected sharp nose flap, and with triangular strakes projecting from the basic wing. The data presented include pressure distributions, wake traverses, boundary-layer traverses, and integrated force and moment coefficients, for each of the leading-edge configurations.

In the discussion, the principal effects produced by the various leading-edge modifications are compared and explained where possible. A comparison is made between calculated and measured pressure distributions.

The results obtained for the basic wing will be discussed more fully in Ref.1, with special reference to leading-edge laminar-separation phenomena.

2 MODEL DETAILS

The 6% thick R.A.E.101 aerofoil spanned the tunnel vertically between turntables in the floor and the ceiling, the centre line of rotation of the turntables coinciding with the 30% chord station of the wing. Pressure plotting was carried out at several chordwise sections near mid-span of the wing.

Planform and sectional views of the wing for the various leading-edge arrangements tested are shown in Figs.1 and 2; Table 1 contains details of the model.

The set of flat triangular strakes at 0.25 wing chord pitch spanwise (see Figs.1(b) and 2(b)) was tested on the basic wing with the pressure-plotting station directly aft of the central strake of a row of seven strakes, and also with the pressure-plotting station midway between the two central strakes of a row of eight strakes.

The sharp leading-edge symmetrical section was derived from the basic R.A.E.101 section by applying a symmetrical 10% chord sharp extension (see Figs.1(d) and 2(d)). A sharp leading-edge section with deflected nose flap was simulated by applying 25° deflection to the sharp extension about a hinge-line which coincided with the leading edge of the basic section (see Fig.2(e)). In each case, a few pressure-plotting holes were available in the leading-edge extension. The isolated strake (see Figs.1(f), 2(f) and 10) was attached to the basic wing at various spanwise positions relative to a mid-span pressure-plotting section.

The tests were made in the R.A.E. No.2 $11\frac{1}{2}$ ft × $8\frac{1}{2}$ ft wind tunnel in November and December, 1955, at a windspeed of 125 ft/sec, giving Reynolds numbers of 1.95×10^6 and 2.15×10^6 in terms of the basic and extended chords respectively.

3 EXPERIMENTAL METHOD

The wing static pressure orifices were connected to multitube manometers. Wake profiles were measured using a pitot comb at high incidences and a traversing pitot at low incidences. The traversing gear was also used to make boundary-layer traverses.

The surface pressure distributions have been integrated to give sectional normal force and pitching-moment coefficients. The wake profiles have been integrated to give sectional profile drag coefficients. The force and moment coefficients have been referred to the basic chord for the tests on the basic wing, and for the tests with strakes attached to the basic wing. For the tests with the sharp extensions attached to the basic wing, the coefficients have been referred to the extended chord.

Blockage corrections have been applied to all the results, using the method of Ref.2. The wing incidence has been corrected for finite-chord tunnel constraint. Incidence corrections to allow for wing twist under load were negligible.

The accuracy of the pressure coefficients and wake traverses is satisfactory. The lift and pitching-moment coefficients are less accurate as the number of pressure-plotting stations near the leading edge was of necessity small* (except for the basic wing). Even so, the results should be adequate to indicate the principal differences between the various sections tested.

4 RESULTS AND DISCUSSION

The results, which are presented in Tables 2-4 and illustrated by Figs.3-15, are intended to provide preliminary data on the principal low-speed effects of some leading-edge modifications to a thin wing. The results for the basic wing will be discussed in more detail in Ref.1.

Table 2 contains chordwise pressure distributions over an incidence range for each of five cases (see Figs.1 and 2), namely:-

(a) on the basic round-nosed symmetrical wing (section R.A.E. 101, 6% t/c);

(b) midway between the two central strakes of a row of eight triangular strakes fitted to the leading edge of (a);

(c) directly aft of the central strake of a row of seven triangular strakes fitted to (a);

(d) on a sharp leading-edge symmetrical section, obtained by applying a 10% chord sharp extension to (a);

(e) on the sharp leading-edge section with nose flap deflected 25°.

The pressure distributions, illustrated by Figs.3(a)-(e), are discussed in para. 4.1. The resulting lift, drag and pitching-moment coefficients, presented in Table 3 and illustrated by Figs.4-7, are discussed in para. 4.2-4.4. The results of the wake traverses are shown in Fig.8 and discussed in para. 4.5. The results of the boundary layer traverses are shown in Figs.9(a)-(e) and discussed in para. 4.6.

In addition to the above tests on the five configurations (a)-(e), pressure distributions were measured with an isolated strake (case (f), see Figs.1 and 10) attached to the basic wing at various distances spanwise from the mid-span pressure-plotting station. The pressure distributions thus obtained are given in Table 4, illustrated by Fig.10, and discussed in para. 4.7.

---

*These tests had to be improvised at short notice.

Fig.11 shows sketches of typical surface flow patterns observed in the course of the tests.

An analysis of the upper surface pressure recovery factors obtained with cases (a), (d) and (f) is given in para. 4.8 and illustrated by Fig.12. A comparison between calculated and measured pressure distributions is made in para. 4.9 for cases (a), (d) and (e), and illustrated by Figs.13-15.

4.1 Chordwise pressure distributions and flow behaviour

The chordwise pressure distributions for the basic round-nosed wing are shown in Fig.3(a). At low incidences, up to and including $\alpha = 5.1^{\circ}$, there was a "short bubble" type of leading-edge separation, in which the separated boundary layer reattaches very close to the point of separation. The presence of such a localised separation was established (to be described in Ref.1) by detailed pressure-plotting traverses near the wing leading edge, which revealed the presence of a very small region of constant pressure on the wing upper surface immediately behind the negative pressure peak. The constant pressure region was too small to be shown on Fig.3(a). The presence of a "short bubble" separation had a negligible effect on the pressure distribution, and the calculated pressure distribution was virtually attained (see para. 4.9). For the sake of clarity, the only "short bubble" curve shown in Fig.3(a) is that for $\alpha = 5.1^{\circ}$.

At some incidence between $\alpha = 5.1^{\circ}$ and $\alpha = 6.1^{\circ}$, the negative pressure peak collapsed suddenly, and the extent of the constant pressure region began to increase as the point of reattachment started to move rearwards on the wing upper surface. This is characteristic of the transition to the "long bubble" type of leading-edge separation. As the incidence was further increased, the bubble lengthened rapidly, see Fig.11(a), the negative pressure peak continued to collapse, and the constant pressure region associated with the bubble spread until it covered virtually the whole wing chord by $\alpha = 12.1^{\circ}$, the wing stalling between $\alpha = 10.1^{\circ}$ and $\alpha = 12.1^{\circ}$. In contrast to the "short bubble," the "long bubble" affected the overall pressure distribution appreciably, even at $\alpha = 6.1^{\circ}$ (see para. 4.9); in addition, the centre-of-pressure position and the sectional profile drag coefficient were affected immediately upon the formation of the long bubble (see para. 4.3 and para. 4.4).

Figs.3(b) and 3(c) show the corresponding pressure distributions for the basic leading edge fitted with a row of triangular strakes. No pressure-plotting points were available on the strake itself, hence Fig.3(c) does not show the pressure distribution on the strake. The pressure distributions obtained midway between the two central strakes of a row of eight strakes, and directly behind the central strake of a row of seven strakes, are similar in character; it will be seen that there was no sudden collapse of the peak negative pressure such as occurred between $\alpha = 5.1^{\circ}$ and $\alpha = 6.1^{\circ}$ on the basic wing. The pressure distributions developed progressively with increasing incidence, without the production of unduly high negative pressures at the wing leading edge.

Visualisation tests, using a suspension of titanium oxide in paraffin, showed (Fig.11) that the addition of the row of strakes to the basic wing entirely changed the type of flow on the upper surface of the wing at incidences where the basic wing regime was of "long bubble" type. On the basic wing, without strakes, the point of reattachment moved rapidly back towards the wing trailing edge as the incidence was increased above $\alpha = 6.1^{\circ}$, and reattachment was not achieved at or above $\alpha = 10.1^{\circ}$. With the row of strakes attached, however, the strong trailing-vortex system shed by the strakes restricted the growth of the "long bubble" with incidence, and the leading-edge separation was confined to small triangular regions, extending

from the portions of the wing leading edge between each pair of adjacent strakes to vertices at 10% chord. Thus, it is reasonable that the effect of the separations on the overall pressure distributions would be less marked than on the basic wing; since the separations were accepted and controlled, rather than avoided altogether, it was inevitable that very high negative pressure peaks would not be obtained at the wing leading edge.

Fig.3(d) shows the pressure distributions obtained with the undeflected sharp leading edge. Since the sharp nose was unable to sustain any negative pressure peak, a leading-edge separation occurred once incidence was applied and was invariably of "long bubble" type. Comparing Figs.3(a) and 3(d), it will be seen that the rate of growth of the "long bubble" was somewhat slower on the sharp section, where the separation started virtually at zero incidence, than on the round-nosed section, where the "long bubble" began between $\alpha = 5.1^\circ$ and $\alpha = 6.1^\circ$. In each case, the constant pressure region had spread to cover the whole wing chord by about $\alpha = 10^\circ$, when the value of the upper surface pressure coefficient was of the order $C_p = -0.5$.

Finally, Fig.3(e) shows the pressure distributions which were obtained for the sharp leading edge with deflected nose flap. Because of the deflected nose flap, there was a lower surface separation from the wing leading edge at $\alpha = 0^\circ$. As the incidence was increased, the extent of this separation diminished. The upper surface pressure distribution developed continuously up to $\alpha = 12.2^\circ$, above which incidence the wing stalled suddenly. It will be shown later (para. 4.2-4.4) that the force and moment characteristics were also altered greatly by the deflection of the nose flap. The effectiveness of the nose flap in postponing the onset of extensive upper-surface separations was due to two factors. Firstly, the repositioning of the main negative pressure peak at the knee of the flap, rather than at the leading edge; this was desirable in view of the sharpness of the leading edge. Secondly, the redistribution of the peak suction over a larger portion of the wing perimeter reduced the magnitude of the negative pressure peak and the adverse pressure gradient which occurred at each incidence; this factor would apply equally well to a round-nosed aerofoil with a deflected nose flap.

4.2 Lift curves

Fig.4 shows the sectional lift curves for the different configurations. The basic wing stalled gently between $\alpha = 10.1^\circ$ and $\alpha = 12.1^\circ$, with $C_{L_{max}} = 0.87$. With a row of strakes added to the basic wing, the wing-incidence curve slope was reduced, but the lift coefficient continued to increase up to 15°, the highest incidence tested. The lift coefficients quoted for the station in line with a strake do not include any contribution from the strake itself, as no static pressure tappings were available on the strake.

The lift-incidence curve obtained with the undeflected sharp leading edge coincided approximately up to 8° with that obtained on the basic wing; the sharp leading edge then stalled with $C_{L_{max}}$ reduced slightly to about 0.8. For the sharp leading edge with the nose flap deflected, the value of the lift coefficient at constant incidence was decreased by about 0.05 at low incidences, but continued to increase up to $\alpha \simeq 13^\circ$, with $C_{L_{max}} \simeq 1.1$. Thus the deflection of the nose flap postponed the stall by about 5°, and increased the value of $C_{L_{max}}$ by about 0.3. Such gains by deflecting nose flaps are typical of any nose-stalling aerofoil. They were probably accentuated in this case because the sharpness of the leading edge made the behaviour of the undeflected case so poor.

4.3 Drag curves

Fig.5 shows the variation of the profile drag coefficient, C_D, with C_L for the same five cases. With the basic round-nosed wing, C_D increased slowly with C_L when the leading-edge separation was of "short bubble" type with virtually instantaneous reattachment. Between $C_L = 0.55$ and $C_L = 0.63$, the leading-edge separation changed to "long bubble" type (see para 4.1) and there was an immediate fifty-fold increase in the value of $\frac{d C_D}{d C_L}$, the higher rate of increase of drag being maintained as the incidence was increased further. Near the stalling incidence, the profile drag coefficient was approximately equal to $C_L \alpha$, showing that all the leading-edge suction forces had been lost.

With the row of strakes attached to the wing, the drag curve measured with the pitot comb directly aft of the central strake was similar to that of the basic section; midway between the two central strakes, the drag coefficient was generally higher at low incidences. In both cases the drag coefficient at constant C_L was higher than on the basic wing, even after the basic wing exhibited a well-developed "long bubble" separation. Thus, although the presence of the strakes confined the "long bubble" to comparatively small areas of the wing, the trailing-vortex for the strakes produced drag coefficients of the same order as those which resulted from the uncontrolled "long bubble" separation*.

With the undeflected sharp leading edge, the drag coefficient increased steadily from $C_L = 0$ to $C_{L_{max}}$, because the "long bubble" started to develop as soon as the incidence was increased from zero. This may be contrasted with the very low rate of drag increase which occurred on the basic wing when the separation was of "short bubble" type, followed by a very rapid increase once the "long bubble" had formed. Below the stall, the profile drag coefficient was less for the basic section; above the stall, when the pressure distributions (see para. 4.1) on the two sections were almost the same, the drag coefficients were approximately equal.

For the sharp leading edge with a deflected nose flap, the drag curve was entirely different from those obtained with the other four configurations. At incidences near zero, the local separation (see para. 4.1) from the wing lower surface caused the profile drag to be increased somewhat; the extent of this separation, and the sectional profile drag coefficient, decreased as the incidence was increased. The value of C_D attained a minimum at $C_L \simeq 0.5$, and the low drag range persisted up to the stall (with $C_D < 0.05$). At the stall, there was a sudden rise in the profile drag coefficient. These are characteristic effects of applying leading-edge camber, or deflecting a nose flap; but the drag reduction due to nose flap deflection was probably accentuated because of the sharp leading edge, which caused large-scale separations in the undeflected case at comparatively low incidences.

4.4 Pitching-moment curves and centre-of-pressure positions

Fig.6 shows C_m v. C_L curves for the different cases, and Fig.7 shows the corresponding variations in centre-of-pressure position. The pitching-moment coefficient is referred to the quarter-chord position. For cases

---

*The integrated drag coefficients quoted for the cases with strakes include some proportion of the induced drag arising from the trailing-vortex system of the strakes; the drag penalty of the strakes would tend to be rather larger than as indicated by the present results.

(a), (b) and (c), the quarter-chord position for the basic wing has been used and the centre-of-pressure, k, is quoted aft of the basic leading edge as a proportion of basic chord. For cases (d) and (e), the quarter-chord position has been based on the extended wing chord (and the coefficients referred to the extended chord); the centre-of-pressure position is quoted from the extended leading edge as a proportion of the extended chord.

With the basic round leading edge, the quarter-chord pitching-moment coefficient remained approximately zero in the "short bubble" regime, and then became increasingly negative (nose-down) as the "long bubble" developed. The centre-of-pressure position meanwhile moved back from 25% chord to 40% chord.

With the row of strakes on the leading edge, the rearward movements of the centre-of-pressure position were reduced.

The undeflected sharp leading edge, behaved in a similar manner to the basic wing, and the total movement of the centre-of-pressure position was again about 15% chord.

The sharp leading edge with the nose flap deflected exhibited a relatively constant negative value of C_m from $C_L = 0$ to $C_L = C_{L_{max}}$, whilst the centre-of-pressure position moved steadily forwards towards the quarter-chord position.

4.5 Wake traverses

The total head deficiency parameter, h, was obtained by expressing the head deficiency as a fraction of the mainstream dynamic head. Fig.8 shows wake profiles for the five configurations measured at one chord (basic) downstream of the wing trailing edge. In the "short bubble" regime up to $\alpha = 5.1^\circ$, the breadth of the wake was 0.1c, with a peak value for h of less than 0.2. But, once the transition to a "long bubble" occurred, both the breadth of the wake and the peak value of h increased; at $C_{L_{max}}$, the wake breadth was about 1.0c and h was of order 0.5. Moreover, the curves obtained with the two types of flow were essentially different in character, the ratio of wake breadth to h_{max} being much higher for the "long bubble" regime.

The wake profiles obtained with the row of strakes attached to the basic wing show an unusual feature at low incidences; both at $\alpha = 3.1^\circ$ (midway between two strakes) and at $\alpha = 5.1^\circ$ (directly aft of a strake), there were two peak values for h. It is considered that the additional peak was associated with the trailing vortices shed by the strakes, particularly since similar effects were found in the boundary layer traverses (see para. 4.6). The curves obtained at higher incidences with the strakes show higher peak values for h and much narrower wakes than were obtained with the basic leading edge; thus, the general shape of the curves was then similar to that obtained with the basic wing at low incidences when the separations were localised near the wing leading edge.

With the undeflected sharp leading edge, only the profile for $\alpha = 0^\circ$ shows the higher ratio of h_{max} to wake breadth which is characteristic of a "short bubble" flow; at the other incidences, the curves obtained showed the lower values of this ratio consistent with a "long bubble" flow. At the higher incidences, the profiles obtained with the sharp and the round leading edges can be seen to be very similar.

In the case of the sharp leading edge with nose flap deflected, however, only the curve for $\alpha = 15.2^\circ$ (above the stall) was of "long bubble"

type and the breadth of the wake was comparatively small at all other incidences. The effect of the lower-surface separation at low incidences can be seen to be small; moreover, this separation did not change the shape of the wake as did the long bubble separations which occurred with the symmetrical round and sharp sections.

4.6 Boundary-layer traverses

The boundary-layer traverses (see Fig.9) for the different leading-edge configurations were generally made for $\alpha = 7.1^{\circ}$, on the wing upper surface at 10%, 35% and 80% chord. The pitot and static traverses were normally made with the head parallel with the local wing surface pointing upstream; when a separated region was present and the velocity fell to zero some distance from the surface, the regions of reversed flow between this point and the surface were examined with the head reversed and pointing downstream. The distance Z was measured normal to the local wing surface with the origin Z = 0 at the wing surface.

At $\alpha = 7.1^{\circ}$, with the basic round-nosed leading edge, the existence of the "long bubble" separation, and the associated reversed flow region, is confirmed (see Fig.9(a)) by the results obtained at about 10% chord. Between 10% and 35% chord, the reversed flow region disappeared; this is consistent with oil and tuft studies (see Fig.11) which indicated reattachment at about 25%-30% chord for this incidence.

With the row of strakes fitted to the leading edge, the traverses midway between and directly aft show large differences. Aft of a strake, it will be seen that the boundary layer was thin, with moderate head losses. Midway between the strakes, the boundary layer height and total head deficiencies were larger, and the results of the traverses were more difficult to interpret. At 5% chord, the existence of reversed flow midway between the strakes was indicated by negative values of U/U_o, with reattachment by 10% chord, this agreed with the results of visualisation tests (see Fig.11), which suggested that the presence of the strakes confined the reversed flow regions to triangular regions extending from the leading edge between adjacent strakes to vertices at 10% chord. The traverses at 35% and 80% chord show two peak values of total head deficiency, one at the surface and the second above the surface. This corresponds to the double peak observed in the wake traverses (para. 4.5) and the additional peak was probably caused by the trailing vortex system created by the strakes.

The traverses at $\alpha = 7.1^{\circ}$ for the symmetrical leading edge (Fig.9(d)) show, as would be expected, the existence of a more extensive separated region than occurred on the basic wing at the same incidence (Fig.9(a)), and the reversed region can be seen to extend further back than 35% chord.

With the nose flap deflected on the sharp leading edge, Fig.9(e), there was no indication of leading-edge separations, either on the lower or on the upper surfaces of the wing at $\alpha = 7.1^{\circ}$; the boundary layer was thin and total head losses small. At $\alpha = 0^{\circ}$, the lower surface separation was revealed by the traverse at 10% chord. This separation was, however, evidently suppressed by $\alpha = 7.1^{\circ}$, and in any case did not result in large profile drag coefficients, even at $\alpha = 0^{\circ}$ (see para. 4.3).

4.7 Pressure distributions at different spanwise distances from an isolated strake

In order to investigate the spanwise distances over which a strake affected the "long bubble" type of separation, some upper-surface pressure distributions were obtained with an isolated strake, see Fig.1(f), attached to the basic wing at various distances from a mid-span pressure traverse. The results are given in Fig.10 for $\alpha = 5.1^{\circ}$, 8.1°, 12.1° and 15.1°.

At $\alpha = 5.1^{\circ}$, the basic wing exhibited a "short bubble" type of flow, and the strake is seen to have had little effect on the wing pressure distribution. At $\alpha = 8.1^{\circ}$, the basic wing (dashed curve) exhibited a "long bubble," with a nearly constant pressure region ($C_p \simeq -1.3$) about 10% chord in extent. With the isolated strake attached to the wing, all the pressure distributions were affected considerably, even as far as 1.067 chord spanwise from the strake; higher negative pressures were obtained at the leading edge, although the general shape of the curves was still that associated with a "long bubble" separation. At $\alpha = 12.1^{\circ}$ and $\alpha = 15.1^{\circ}$, the same trend can be seen. In these cases, the basic wing had a constant region occupying the whole wing chord, the presence of the strake created extensive regions near the wing leading edge where the pressure was more negative than on the basic wing. As at $\alpha = 8.1^{\circ}$, the presence of the strake caused significant changes in the upper surface pressure distributions as much as 1.067 chord spanwise from the strake.

Flow visualisation studies, using titanium oxide, confirmed (Fig.11) that the isolated strake affected the surface flow for a considerable distance spanwise. At $\alpha = 8.1^{\circ}$, where reattachment occurred on the basic wing at about 40% chord, the isolated strake caused the reattachment position to move forward to the leading edge in the vicinity of the strake; the new reattachment line swept back to blend into the normal constant-chord reattachment position at about 0.5 chord spanwise from the strake. At $\alpha = 12.1^{\circ}$ and $\alpha = 15.1^{\circ}$, the basic wing exhibited a complete separation; the addition of the strake created a reattachment line sweeping downstream from the strake to the wing trailing edge at about 0.5 chord spanwise from the strake. Thus, the presence of the strake affected the surface flow considerably at distances of the order 0.5 chord spanwise from the strake, and it does not seem unreasonable that the effect on the pressure distribution should extend still further from the strake.

4.8 Pressure recovery factors

In Ref.3, Norbury and Crabtree have considered the pressure recovery region of a "long bubble." A pressure recovery factor, σ, is defined by $\sigma = \frac{C_{p_2} - C_{p_1}}{1 - C_{p_1}}$ where C_{p_2} is the pressure coefficient at the reattachment position and C_{p_1} is the virtually constant pressure coefficient over the front of the bubble. By applying the momentum theorem and the equation of continuity to the pressure recovery region, it is shown that the value of σ should lie between 0.37 and 0.45, provided reattachment occurs ahead of the wing trailing edge. When reattachment is near the trailing edge, or does not occur at all, part or all of the pressure recovery takes place in the wake; in such cases, the trailing-edge pressure can be used for C_{p_2} but σ tends to be smaller than the above values. The experimental evidence of Ref.4 was shown to support the theory.

Fig.12 shows the trends for the present tests. Although it is difficult to assign the value of C_{p_2} accurately, the general trends presented should be correct.

The top diagram shows the variation of σ with α for the basic round leading edge and for the undeflected sharp leading edge. The value of σ decreases with increasing wing incidence, falling to zero above the stall when all the pressure recovery took place in the wake aft of the wing trailing edge. At constant incidence below the stall, σ is smaller for the sharp section because of the larger degree of separation.

The lower diagram shows the spanwise variation of σ for three incidences with an isolated strake attached to the basic wing. The strake tends to increase the value of σ, particularly at the two higher incidences, where the influence of the strake extends over one chord length spanwise from the centre of the strake.

4.9 Comparison between measured and calculated pressure distributions

Figs.13, 14 and 15 show, for comparison, measured and calculated pressure distributions for cases (a), (d) and (e) at various incidences. The theoretical distributions have been calculated using Refs.5 and 6, no allowance having been made for the effect of the separations on the calculated distributions. For the basic wing at $\alpha = 5.1^{\circ}$, there is good agreement between measured and calculated pressure distributions (see Fig.13), because the presence of the short bubble had only local effects on pressure distribution. However, between $\alpha = 5.1^{\circ}$ and $\alpha = 6.1^{\circ}$, the "long bubble" formed with an immediate effect on the experimental distribution. The peak suction at the leading edge collapsed; and, instead, there was a region of nearly constant pressure occupying about 5% chord. As the incidence increased further, see Fig.3(a), the "long bubble" developed and affected the measured pressure distributions progressively.

With the undeflected sharp leading edge, the "long bubble" separation began as soon as the wing incidence increased from zero, thus causing large effects on the pressure distribution, even at $\alpha = 3.1^{\circ}$ (see Fig.14).

Finally, in the case of the sharp leading edge with nose flap deflected 25° (see Fig.15), the calculated and measured pressure distributions differ considerably at $\alpha = 0^{\circ}$ and $\alpha = 3.1^{\circ}$, as a result of the lower-surface separation. From $\alpha = 5.1^{\circ}$ to $\alpha = 12.2^{\circ}$, the differences between experiment and calculation are not large, although the predicted double peak in the upper-surface pressure distribution was not attained in practice. This was probably due to a local separation from the sharp leading edge* on the upper surface, which was confined by the favourable pressure gradient ahead of the second peak at the knee of the flap. (However, the number of pressure-plotting stations near the leading edge was not sufficient for this to be stated with certainty.) This leading edge showed no marked separations below $\alpha = 12.2^{\circ}$, and thus good agreement was obtained over virtually the whole of the incidence range right up to the stall.

It is clear that a theoretical method for calculating the pressure distributions which would occur on a thin wing should make due allowance for the effects of the leading-edge separations. Such a method has been proposed by Maskell[8], which yields an infinity of possible solutions, since the pressure head in the bubble is arbitrary. However, if an appropriate value for σ can be assigned (see Ref.3 and para. 4.8), then the solution becomes determinate. An example calculated by this method is given in Ref.9, and this shows good agreement with the pressure distribution measured on a wing with a "long bubble" present.

5 CONCLUSIONS

At the test Reynolds number (2×10^6), the upper surface of the basic round-nosed section exhibited a "short bubble" flow up to 5° incidence, above which incidence a "long bubble" developed, spreading to the trailing edge by 10° ($C_{L_{max}} = 0.87$).

---

*When a nose flap is deflected on a thin round-nosed section (e.g., see Ref.7), the theoretical double peak distribution is attained in practice.

Addition of a spanwise row of triangular strakes along the leading edge inhibited the bubble growth, and allowed a certain degree of peak negative pressure to occur near the leading edge. However, with the particular strake arrangement tested, the lift-incidence curve slope was reduced, $C_{L_{max}}$ was not increased, and the overall drag coefficient at a given lift coefficient was not reduced.

Addition of a sharp leading edge to the basic round nose caused a "long bubble" flow to develop from immediately above zero incidence, resulting in an early stall ($C_{L_{max}} = 0.8$).

On deflection of a nose flap with this sharp leading edge, the upper surface flow remained attached, with some evidence of local separation and reattachment on the surface of the deflected nose, right up to the stall; C_L was decreased slightly at low incidences but the lift curve was extended ($C_{L_{max}} \simeq 1.1$).

The measured profile drag coefficients reflected the formation and development of the "long bubble". Loss of the leading-edge suction peak on the formation of such a bubble, resulted in rapid increase of drag. This change took place at 5° on the basic round-nosed section, and at 0° with the sharp nose; when the sharp nose was deflected the drag remained low right up to the stall.

Observed movement of the centre-of-pressure position, and changes in the wake shape and boundary-layer profiles, were likewise found to be associated with the development of the bubble flows.

Some additional tests on the basic round-nosed section showed that a single small strake fitted to the leading edge substantially affected the bubble formation for a spanwise distance in excess of one wing-chord length from the strake.

NOTATION

c	basic chord
$c_e = 1.1c$	extended chord
C_D	drag coefficient
C_L	lift coefficient
C_m	pitching moment coefficient
C_p	surface pressure coefficient
C_{p_1}	constant value of C_p in fore portion of long-bubble
C_{p_2}	value of C_p at reattachment position
$h = \frac{H_o - H}{H_o - p_o}$	wake total head deficiency coefficient
h_{max}	maximum value of h across the wake

H	total head
H_o	tunnel total head
k	distance of centre-of-pressure position on wing from leading edge
p	static pressure
p_o	tunnel static pressure
U	local velocity in boundary layer
U_o	mainstream velocity
$\frac{U}{U_o} = \sqrt{\frac{H-p}{H_o-p_o}}$	ratio of local velocity in boundary-layer to mainstream velocity
x	chordwise distance from leading edge
z	normal distance from local surface in boundary-layer traverses
Z	distance from tunnel centre-line in wake traverses (see Fig.8)
α	wing incidence
$\sigma = \frac{C_{p_2} - C_{p_1}}{1 - C_{p_1}}$	pressure recovery factor

---

LIST OF REFERENCES

No.	Author	Title, etc.
1	Butler, S.F.J.	Low speed tests on a 6% thick R.A.E. aerofoil section. R.A.E. Report to be issued.
2	Maskell, E.C.	Theory of wind tunnel blockage effects on stalled flows. R.A.E. Report to be issued.
3	Norbury, J.F. Crabtree, L.F.	A simplified model of the incompressible flow past two-dimensional aerofoils with a long bubble type of flow separation. R.A.E. Tech. Note No. Aero 2352. June, 1955. A.R.C. 17945.
4	McCullough, G.B. Gault, D.E.	Examples of three representative types of airfoil-section stall at low speed. September, 1951. N.A.C.A. T.N. No. 2502.

LIST OF REFERENCES (Contd.)

No.	Author	Title, etc.
5	Weber, J.	The calculation of the pressure distribution over the surface of two-dimensional and swept wings with symmetrical aerofoil sections. R.A.E. Report No. Aero 2497. R & M 2918 July, 1953.
6	Weber, J.	The calculation of the pressure distribution on the surface of thick cambered wings and the design of wings with given pressure distributions. R.A.E. Report No. Aero 2598. June, 1955.
7	Gambucci, B.J.	Section characteristics of the N.A.C.A. 0006 airfoil with leading-edge and trailing-edge flaps. December, 1956. N.A.C.A. T.N. No. 3797.
8	Maskell, E.C.	A theoretical treatment of the thin-aerofoil stall. R.A.E. Report to be issued.
9	Crabtree, L.F.	Effects of leading-edge separations on thin wings in two-dimensional incompressible flow. Journal of the Aeronautical Sciences, Vol. 24 pp. 597-604. August, 1957.

TABLE 1

Model details

Wind tunnel R.A.E. No.2 $11\frac{1}{2}$ ft × $8\frac{1}{2}$ ft

Configuration	(a) Round leading edge	(d) Sharp leading edge
Span	8.5 ft spanning tunnel vertically	
Chord	c = 2.5 ft	c_e = 2.75 ft
Section	R.A.E. 101	R.A.E. 101 + 10% leading edge extension
t/c	0.06	0.054
Max. thickness position	0.3 chord	0.36 extended chord
Test Reynolds number	1.95×10^6	2.15×10^6

Details of strakes

Several arrangements of strakes were tested on (a), the basic round-nosed section, namely:-

(b) A row of 8 strakes at 7.5 in. pitch spanwise (0.25c).
(c) A row of 7 strakes at 7.5 in. pitch spanwise (0.25c).

For cases (b) and (c), the planform of each strake was an isosceles triangle, of base 3.2 in. (0.107c) and height 4.8 in. (0.16c) (see Fig.1).

(f) An isolated strake at various spanwise distances from a static pressure traverse.

For case (f), the planform of the strake was a symmetrical trapezoid of height 3.2 in. (0.107c) and parallel sides of lengths 1.07, 3.2 in. (0.036c, 0.107c) (see Figs.1 and 10).

TABLE 2

Surface pressure coefficients

(a) Round leading edge

U_o = 125 ft/sec R = 1.95×10^6

	x/c \ α	0	5.1	6.1	8.1	10.1	12.1	15.1
Wing upper surface	0	+0.990	-3.363	-2.071	-1.775	-1.640	-0.663	-0.713
	0.0048	0.033	-3.801	-1.933	-1.548	-1.372	-0.481	-0.472
	0.0116	-0.093	-1.950	-1.966	-1.559	-1.387	-0.483	-0.474
	0.0488	-0.160	-1.094	-1.950	-1.573	-1.316	-0.481	-0.468
	0.099	-0.183	-0.794	-1.245	-1.380	-0.937	-0.481	-0.466
	0.199	-0.187	-0.570	-0.588	-1.053	-0.810	-0.498	-0.474
	0.299	-0.184	-0.460	-0.474	-0.814	-0.788	-0.514	-0.478
	0.397	-0.151	-0.375	-0.393	-0.595	-0.743	-0.524	-0.486
	0.498	-0.117	-0.304	-0.342	-0.429	-0.688	-0.531	-0.492
	0.597	-0.081	-	-	-	-	-	-
	0.697	-0.037	-0.157	-0.173	-0.229	-0.532	-0.533	-0.531
	0.797	-0.004	-0.091	-0.106	-0.168	-0.444	-0.537	-0.551
	0.899	+0.029	-0.027	-0.045	-0.109	-0.364	-0.527	-0.549
	0.969	0.074	+0.040	+0.031	-0.073	-0.299	-0.477	-0.499
Wing lower surface	0.0044	+0.139	+0.960	+0.976	+0.956	+0.945	+0.980	+0.973
	0.0114	-0.069	0.910	0.920	0.958	0.963	0.956	1.005
	0.060	-0.154	0.487	0.531	0.605	0.643	0.644	0.728
	0.099	-0.163	0.354	0.398	0.474	0.510	0.513	0.603
	0.199	-0.184	0.184	0.221	0.290	0.324	0.325	0.410
	0.300	-0.179	0.103	0.136	0.188	0.225	0.226	0.290
	0.399	-0.154	0.075	0.100	0.143	0.165	0.160	0.216
	0.498	-0.117	0.059	0.081	0.114	0.124	0.106	0.155
	0.598	-0.077	0.061	0.074	0.095	0.101	0.062	0.102
	0.698	-0.026	0.061	0.072	0.080	0.065	0.025	0.048
	0.798	-0.009	0.061	0.060	0.059	0.024	-0.050	-0.026
	0.899	+0.029	0.066	0.059	0.033	-0.030	-0.133	-0.126
	0.971	+0.059	0.069	0.054	-0.008	-0.115	-0.222	-0.272

TABLE 2 (Contd.)

Surface pressure coefficients

(b) Round leading edge - midway between strakes

U_o = 125 ft/sec R = 1.95×10^6

	α / x/c	0	5.1	7.1	10.1	12.1	15.1
Wing upper surface	0	+1.006	-1.309	-1.873	-2.497	-2.420	-2.141
	0.0048	0.074	-1.391	-1.597	-2.140	-2.206	-2.114
	0.0116	-0.065	-1.464	-1.661	-2.186	-2.276	-2.166
	0.0488	-0.150	-1.293	-1.601	-1.600	-1.630	-1.466
	0.099	-0.173	-0.602	-0.882	-1.237	-1.274	-1.287
	0.199	-0.182	-0.552	-0.706	-0.867	-0.928	-0.991
	0.299	-0.182	-0.406	-0.539	-0.695	-0.759	-0.816
	0.397	-0.150	-0.336	-0.429	-0.565	-0.610	-0.645
	0.498	-0.104	-0.267	-0.333	-0.433	-0.477	-0.513
	0.597	-0.072	-0.199	-0.251	-0.334	-0.381	-0.432
	0.697	-0.039	-0.137	-0.176	-0.286	-0.315	-0.385
	0.797	-0.014	-0.085	-0.119	-0.191	-0.252	-0.347
	0.899	+0.018	-0.026	-0.057	-0.129	-0.198	-0.309
	0.969	0.062	+0.033	+0.002	-0.082	-0.158	-0.289
Wing lower surface	0		-1.203	-1.710	-2.392	-2.579	-2.358
	0.0048		+1.009	+0.914	+0.738	+0.650	+0.551
	0.0116		0.923	0.978	1.005	1.001	0.976
	0.0488		0.513	0.640	0.774	0.809	0.849
	0.099		0.318	0.428	0.552	0.589	0.638
	0.199		0.168	0.262	0.354	0.377	0.420
	0.299		0.095	0.173	0.219	0.256	0.286
	0.397		0.070	0.131	0.183	0.186	0.199
	0.498		0.056	0.099	0.145	0.137	0.137
	0.597		0.059	0.096	0.118	0.103	0.090
	0.697		0.065	0.092	0.080	0.070	0.044
	0.797		0.065	0.078	0.062	0.027	-0.014
	0.899		0.065	0.067	0.033	0.007	-0.085
	0.969		0.070	0.058	0.001	-0.058	-0.150

TABLE 2 (Contd.)

Surface pressure coefficients

(c) Round leading edge - directly aft of strake

U_o = 125 ft/sec R = 1.95×10^6

	x/c \ α	0	5.1	7.1	10.1	12.1	15.1
Wing upper surface	0	+0.496	+0.319	+0.746	+0.226	+0.215	+0.120
	0.0048	0.307	-0.042	-0.148	-0.127	-0.194	-0.307
	0.0116	0.085	-0.454	-0.613	-0.608	-0.721	-0.825
	0.0488	-0.127	-0.709	-0.865	-1.184	-1.352	-1.265
	0.099	-0.159	-0.640	-0.851	-1.162	-1.172	-1.151
	0.199	-0.171	-0.532	-0.673	-0.863	-0.897	-0.947
	0.299	-0.168	-0.468	-0.575	-0.731	-0.771	-0.789
	0.397	-0.143	-0.383	-0.465	-0.585	-0.626	-0.630
	0.498	-0.106	-0.295	-0.356	-0.455	-0.500	-0.520
	0.597	-0.074	-0.215	-0.267	-0.350	-0.401	-0.459
	0.697	-0.041	-0.148	-0.191	-0.271	-0.333	-0.432
	0.797	-0.016	-0.093	-0.130	-0.204	-0.277	-0.378
	0.899	+0.019	-0.033	-0.066	-0.143	-0.214	-0.333
	0.969	0.058	+0.034	-0.002	-0.093	-0.166	-0.298
Wing lower surface	0		+0.766	+0.832	+0.880	+0.901	+0.924
	0.0048		0.732	0.818	0.878	0.894	0.924
	0.0116		0.596	0.712	0.802	0.829	0.873
	0.0488		0.418	0.548	0.658	0.691	0.743
	0.099		0.294	0.414	0.517	0.548	0.603
	0.199		0.171	0.262	0.345	0.365	0.402
	0.299		0.100	0.169	0.235	0.242	0.265
	0.397		0.071	0.126	0.177	0.198	0.187
	0.498		0.059	0.105	0.137	0.126	0.127
	0.597		0.062	0.092	0.110	0.111	0.073
	0.697		0.055	0.074	0.088		0.031
	0.797		0.059	0.069	0.056	0.021	-0.030
	0.899		0.059	0.053	0.018	-0.028	-0.099
	0.969		0.073	0.051	-0.013	-0.072	-0.175

TABLE 2 (Contd.)

Surface pressure coefficients

(d) Sharp leading edge

U_o = 125 ft/sec R = 2.15×10^6

	α / x/c_e*	0	1.0	2.0	3.1	4.1	5.1	6.1	7.1	10.2	12.2	15.2
Wing upper surface	0.0455	+0.083	-0.018	-0.783	-1.047	-0.912	-1.153	-1.079	-0.937	-0.630	-0.518	-0.530
	0.0919	0.019	-0.068	-	-0.793	-1.150	-1.185	-1.096	-0.952	-0.643	-0.527	-0.532
	0.181	-0.234	-0.306	-0.350	-	-0.475	-0.883	-1.050	-0.958	-0.667	-0.555	-0.538
	0.272	-0.155	-0.215	-0.270	-0.298	-0.310	-0.482	-0.891	-0.952	-0.720	-0.592	-0.540
	0.362	-0.169	-0.212	-0.258	-0.289	-0.299	-0.315	-0.590	-0.817	-0.742	-0.615	-0.550
	0.452	-0.146	-0.180	-0.219	-0.250	-0.262	-0.260	-0.375	-0.651	-0.748	-0.628	-0.557
	0.544	-0.110	-0.141	-0.171	-0.195	-0.212	-0.210	-0.255	-0.493	-0.715	-0.632	-0.567
	0.634	-0.077	-0.100	-0.125	-0.147	-0.161	-0.162	-0.184	-0.352	-0.671	-0.620	-0.579
	0.725	-0.041	-0.059	-0.081	-0.096	-0.113	-0.112	-0.129	-0.248	-0.610	-0.604	-0.604
	0.816	-0.013	-0.031	-0.047	-0.057	-0.069	-0.071	-0.088	-0.171	-0.529	-0.581	-0.629
	0.909	+0.017	+0.003	-0.003	-0.004	-0.019	-0.023	-0.044	-0.108	-0.439	-0.525	-0.594
	0.972	0.060	0.051	+0.045	+0.046	+0.054	+0.021	-0.003	-0.069	-0.362	-0.449	-0.538
Wing lower surface	0.0455		+0.227	+0.355	+0.457	+0.542	+0.621		+0.694	+0.745	+0.766	+0.842
	0.091		0.120	0.223	0.303	0.372	0.439		0.515	0.463	0.598	0.685
	0.181		-0.114	-0.076	-0.003	0.061	0.128		0.217	0.272	0.305	0.410
	0.272		-0.086	-0.024	+0.033	0.082	0.132		0.199	0.239	0.264	0.358
	0.362		-0.109	-0.060	-0.008	0.027	0.069		0.130	0.156	0.171	0.259
	0.452		-0.098	-0.055	-0.019	0.013	0.048		0.092	0.110	0.113	0.193
	0.544		-0.075	-0.042	-0.006	0.016	0.041		0.080	0.073	0.075	0.143
	0.634		-0.050	-0.024	+0.001	0.020	0.044		0.069	0.047	0.035	0.091
	0.725		-0.020	-0.001	0.021	0.034	0.051		0.067	0.025	0.001	0.048
	0.816		-0.004	+0.013	0.026	0.034	0.044		0.049	-0.019	-0.061	-0.022
	0.909		+0.024	0.031	0.042	0.041	0.046		0.033	-0.080	-0.153	-0.126
	0.972		0.060	0.065	0.067	0.059	0.062		0.018	-0.157	-0.259	-0.243

* $\frac{x}{c_e}$ based on extended chord, c_e

TABLE 2 (Contd.)

Surface pressure coefficients

(e) Sharp leading edge - nose flap deflected 25°

U_o = 125 ft/sec R = 2.15×10^6

	α / x^*/c_e	0	3.1	5.1	7.1	10.2	12.2	15.2
Wing upper surface	0.0455	+0.383	-0.045	-0.409	-0.687	-2.922	-3.368	-1.160
	0.076	-0.087	-0.583	-0.997	-1.328	-1.679	-2.727	-1.176
	0.181	-	-0.365	-0.559	-0.746	-0.997	-1.130	-1.038
	0.272	-0.220	-0.425	-0.552	-0.685	-0.842	-0.892	-1.047
	0.362	-0.213	-0.372	-0.470	-0.567	-0.685	-	-0.983
	0.452	-0.177	-0.303	-0.377	-0.456	-0.546	-0.570	-0.914
	0.544	-0.136	-0.236	-0.292	-0.352	-0.421	-0.445	-0.833
	0.634	-0.099	-0.176	-0.219	-0.265	-0.324	-0.345	-0.740
	0.725	-0.058	-0.121	-0.149	-0.182	-0.230	-0.259	-0.642
	0.816	-0.035	-0.079	-0.099	-0.120	-0.160	-0.193	-0.550
	0.909	+0.003	-0.020	-0.030	-0.039	-0.076	-0.127	-0.455
	0.972	0.040	+0.040	+0.038	+0.034	-0.008	-0.048	-0.292
Wing lower surface	0.0455	-0.545	-0.015	+0.484	+0.651	+0.805	+0.861	+0.839
	0.076	-0.554	+0.001	0.617	0.690	0.817	0.854	0.848
	0.182	-0.413	0.187	0.166	0.217	0.316	0.397	0.395
	0.272	-0.049	0.095	0.171	0.274	0.385	0.434	0.434
	0.364	-0.017	0.024	0.100	0.185	0.282	0.322	0.322
	0.453	-0.049	0.003	0.070	0.143	0.223	0.254	0.249
	0.544	-0.049	0.003	0.058	0.123	0.186	0.206	0.189
	0.635	-0.033	0.013	0.056	0.109	0.154	0.172	0.138
	0.726	-0.015	0.026	0.065	0.100	0.136	0.143	0.096
	0.817	+0.004	0.031	0.056	0.088	0.106	0.102	0.030
	0.909	0.026	0.045	0.063	0.077	0.076	0.056	-0.057
	0.974	0.060	0.068	0.072	0.075	0.054	0.015	-0.158

$\frac{x^*}{c_e}$ based on extended chord, c_e

TABLE 3

Lift, drag and pitching moment coefficients and centre of pressure positions

(a) Round leading edge

U_o = 125 ft/sec R = 1.95×10^6

α	C_L	C_D	C_m	$\frac{k}{c}$
0	0	+0.005	0	-
+5.1	+0.544	0.0085	+0.001	+0.248
6.1	0.629	0.042	-0.001	0.251
8.1	0.777	0.114	-0.018	0.273
10.1	0.868	0.191	-0.088	0.349
12.1	0.646	0.237	-0.102	0.399
15.1	0.656	0.273	-0.099	0.390

(b) Round leading edge - midway between strakes

U_o = 125 ft/sec R = 1.95×10^6

α	C_L	C_D	C_m	$\frac{k}{c}$
0	0	+0.0095	0	-
+3.1	-	0.030	-	-
5.1	+0.486	0.056	-0.004	+0.258
7.1	0.631	0.084	-0.015	0.273
10.1	0.801	0.141	-0.026	0.282
12.1	0.840	0.168	-0.031	0.286
15.1	0.865	-	-0.046	0.302

(c) Round leading edge - directly aft of strake

U_o = 125 ft/sec R = 1.95×10^6

α	C_L	C_D	C_m	$\frac{k}{c}$
0	0	+0.0115	0	-
+3.1	-	0.007	-	-
5.1	+0.427	0.021	-0.020	+0.298
7.1	0.557	0.068	-0.029	0.301
10.1	0.708	0.128	-0.040	0.305
12.1	0.772	0.155	-0.043	0.305
15.1	0.806	-	-0.050	0.310

TABLE 3 (Contd.)

(d) Sharp leading edge*

U_o = 125 ft/sec R = 2.15×10^6

α	C_L	C_D	C_m	$\frac{k}{c}$
0	0	+0.0105	0	-
+3.1	+0.354	0.0235	+0.001	+0.248
4.1	0.407	-	0.001	0.247
5.1	0.524	0.049	0.006	0.238
7.1	0.731	0.105	-0.044	0.309
10.2	0.759	0.211	-0.110	0.390
12.2	0.703	-	-0.103	0.391
15.2	0.757	0.224	-0.120	0.402

(e) Sharp leading edge - nose flap deflected 25°*

U_o = 125 ft/sec R = 2.15×10^6

α	C_L	C_D	C_m	$\frac{k}{c}$
0	-0.045	+0.026	-0.035	-0.533
+3.1	+0.264	0.0145	-0.035	+0.381
5.1	0.495	0.0125	-0.021	0.299
7.1	0.670	0.0145	-0.031	0.299
10.2	0.969	0.030	-0.020	0.271
12.2	1.091	0.048	-0.016	0.265
15.2	1.077	0.240	-0.123	0.362

*Coefficients based on extended chord, c_e

TABLE 4

Upper surface pressure coefficients

(f) Round leading edge - at different spanwise stations relative to a single strake

U_o = 12.5 ft/sec R = 1.95×10^6

Location of traverse	$\frac{x}{c}$ \ α	5.1	6.1	8.1	10.1	12.1	15.1
0.067c spanwise from centre-line of strake	0	-2.859	-3.448	-3.092	-2.280	-2.959	-3.806
	0.0048	-3.101	-3.372	-2.530	-1.853	-2.421	-1.937
	0.0116	-1.450	-1.679	-2.510	-1.820	-1.997	-1.444
	0.0488	-1.018	-1.732	-2.309	-1.924	-1.963	-1.595
	0.099	-0.806	-1.330	-1.763	-1.573	-1.202	-0.767
	0.199	-0.515	-0.591	-0.825	-0.848	-0.581	-0.485
	0.299	-0.409	-0.422	-0.571	-0.689	-0.575	-0.489
	0.397	-0.342	-0.361	-0.462	-0.611	-0.601	-0.515
	0.498	-0.279	-0.296	-0.370	-0.534	-0.609	-0.540
	0.597	-	-	-	-	-	-
	0.697	-0.141	-0.154	-0.204	-0.384	-0.616	-0.591
	0.797	-0.083	-0.094	-0.138	-0.317	-0.580	-0.608
	0.899	-0.023	-0.037	-0.071	-0.247	-0.532	-0.602
	0.969	+0.044	+0.037	+0.002	-0.180	-0.460	-0.561
0.167c spanwise from centre-line of strake	0	-2.414	-1.936	-2.281	-2.085	-2.114	-1.718
	0.0048	-2.633	-1.767	-1.832	-1.672	-1.739	-1.439
	0.0116	-2.097	-1.802	-1.852	-1.679	-1.756	-1.444
	0.0488	-1.162	-1.781	-1.935	-1.679	-1.806	-1.495
	0.099	-0.722	-1.145	-1.531	-1.322	-1.250	-1.067
	0.199	-0.552	-0.759	-0.918	-0.985	-1.114	-0.874
	0.299	-0.445	-0.506	-0.715	-0.797	-0.590	-0.640
	0.397	-0.371	-0.412	-0.559	-0.665	-0.566	-0.567
	0.498	-0.306	-0.326	-0.410	-0.568	-0.562	-0.558
	0.597	-	-	-	-	-	-
	0.697	-0.180	-0.171	-0.225	-0.409	-0.575	-0.579
	0.797	-0.119	-0.107	-0.159	-0.338	-0.555	-0.569
	0.899	-0.050	-0.043	-0.100	-0.268	-0.508	-0.530
	0.969	+0.016	+0.019	-0.033	-0.206	-0.441	-0.479

TABLE 4 (Contd.)

Location of traverse	$\frac{x}{c}$ \ α	5.1	6.1	8.1	12.1	15.1
0.267c spanwise from centre-line of strake	0	-3.373	-1.879	-2.020	-1.760	-1.532
	0.0048	-3.809	-1.837	-1.600	-1.394	-1.288
	0.0116	-1.937	-1.741	-1.597	-1.396	-1.292
	0.0488	-1.078	-1.764	-1.665	-1.433	-1.335
	0.099	-0.781	-1.307	-1.649	-1.394	-1.370
	0.199	-0.556	-0.588	-0.983	-1.029	-0.808
	0.299	-0.445	-0.454	-0.603	-0.791	-0.691
	0.397	-0.364	-0.381	-0.467	-0.657	-0.644
	0.498	-0.293	-0.312	-0.367	-0.542	-0.569
	0.597	-	-	-	-	-
	0.697	-0.146	-0.169	-0.214	-0.493	-0.550
	0.797	-0.089	-0.109	-0.153	-0.454	-0.542
	0.899	-0.023	-0.049	-0.099	-0.385	-0.501
	0.969	+0.033	-0.001	-0.056	-0.294	-0.444
0.467c spanwise from centre-line of strake	0	-3.401	-2.138	-1.595	-1.567	-1.310
	0.0048	-3.836	-1.973	-1.254	-1.221	-1.186
	0.0116	-1.959	-2.000	-1.256	-1.229	-1.194
	0.0488	-1.095	-1.966	-1.308	-1.238	-1.192
	0.099	-0.794	-1.115	-1.369	-1.227	-1.205
	0.199	-0.570	-0.575	-1.177	-1.032	-1.056
	0.299	-0.456	-0.462	-0.761	-0.739	-0.769
	0.397	-0.371	-0.403	-0.490	-0.624	-0.626
	0.498	-0.301	-0.301	-0.347	-0.588	-0.600
	0.597	-	-	-	-	-
	0.697	-0.153	-0.159	-0.196	-0.510	-0.550
	0.797	-0.088	-0.099	-0.137	-0.440	-0.492
	0.899	-0.023	-0.039	-0.088	-0.345	-0.399
	0.969	+0.039	+0.011	-0.051	-0.258	-0.313

TABLE 4 (Contd.)

Location of traverse	$\frac{x}{c}$ \ α	5.1	6.1	8.1	10.1	12.1	15.1
0.767c spanwise from centre-line of strake	0	-3.302	-2.111	-2.287	-	-1.703	-1.248
	0.0048	-3.378	-1.936	-1.840	-	-1.372	-0.994
	0.0116	-1.914	-1.945	-1.874	-	-1.392	-1.017
	0.0488	-1.087	-1.945	-1.898	-	-1.349	-1.052
	0.099	-0.787	-1.196	-1.387	-	-1.059	-0.827
	0.199	-0.568	-0.573	-0.917	-	-0.849	-0.693
	0.299	-0.454	-0.462	-0.718	-	-0.832	-0.693
	0.397	-0.372	-0.382	-0.534	-	-0.752	-0.688
	0.498	-0.300	-0.306	-0.397	-	-0.698	-0.670
	0.597	-	-	-	-	-	-
	0.697	-0.155	-0.159	-0.218	-	-0.542	-0.569
	0.797	-0.095	-0.099	-0.154	-	-0.456	-0.503
	0.899	-0.028	-0.042	-0.104	-	-0.376	-0.438
	0.969	+0.041	+0.016	-0.068	-	-0.311	-0.383
1.067c spanwise from centre-line of strake	0	-3.362	-2.114	-2.311	-1.999	-1.416	-1.041
	0.0048	-3.793	-1.943	-1.859	-1.586	-1.120	-0.751
	0.0116	-1.939	-1.968	-1.875	-1.591	-1.120	-0.739
	0.0488	-1.091	-1.945	-1.918	-1.525	-1.079	-0.816
	0.099	-0.792	-1.170	-1.389	-1.113	-0.793	-0.610
	0.199	-0.564	-0.567	-0.915	-0.878	-0.691	-0.593
	0.299	-0.456	-0.456	-0.739	-0.827	-0.702	-0.618
	0.397	-0.368	-0.376	-0.546	-0.621	-0.706	-0.640
	0.498	-0.299	-0.301	-0.408	-0.627	-0.687	-0.644
	0.597	-	-	-	-	-	-
	0.697	-0.147	-0.152	-0.221	-0.441	-0.590	-0.595
	0.797	-0.085	-0.091	-0.162	-0.361	-0.547	-0.554
	0.899	-0.021	-0.031	-0.108	-0.289	-0.469	-0.497
	0.969	+0.044	+0.026	-0.074	-0.243	-0.392	-0.442

WT.2078.C.P.410.K3 - Printed in Great Britain

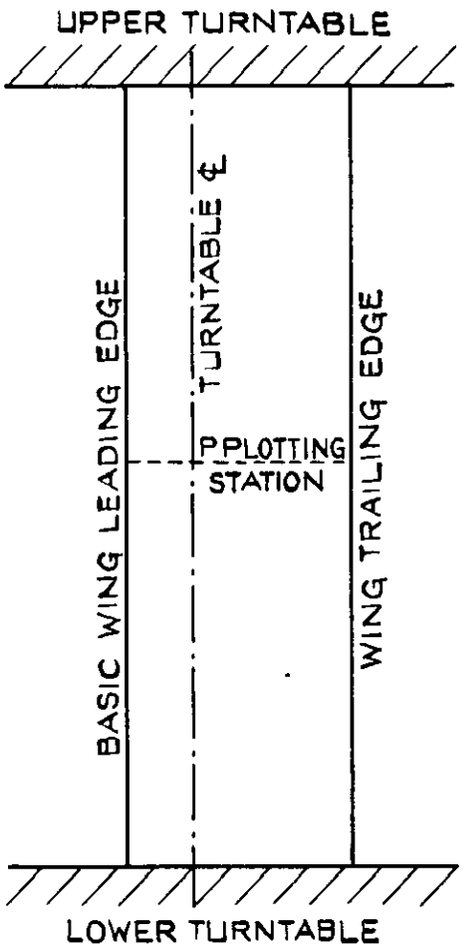

(a) ROUND LEADING EDGE

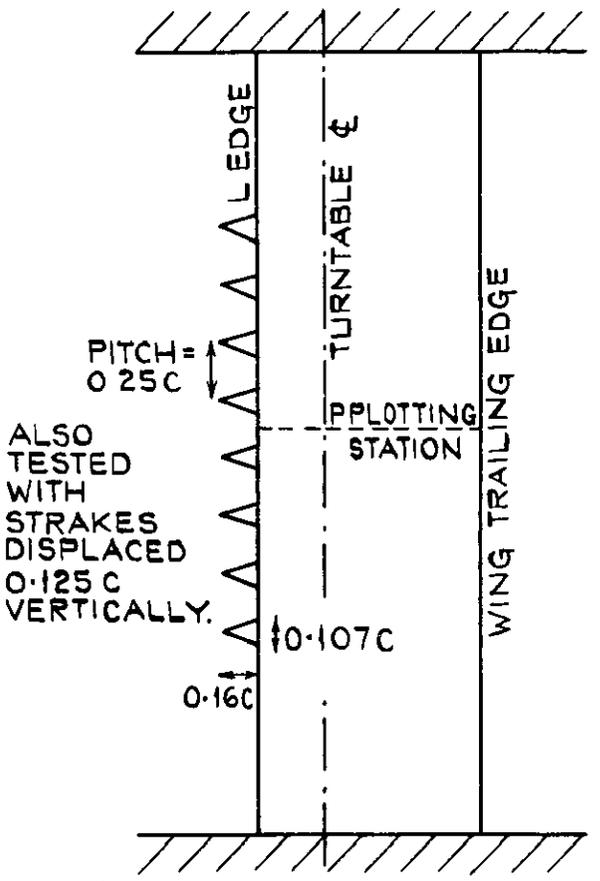

(b), (c) ROUND LEADING EDGE – STRAKES ON

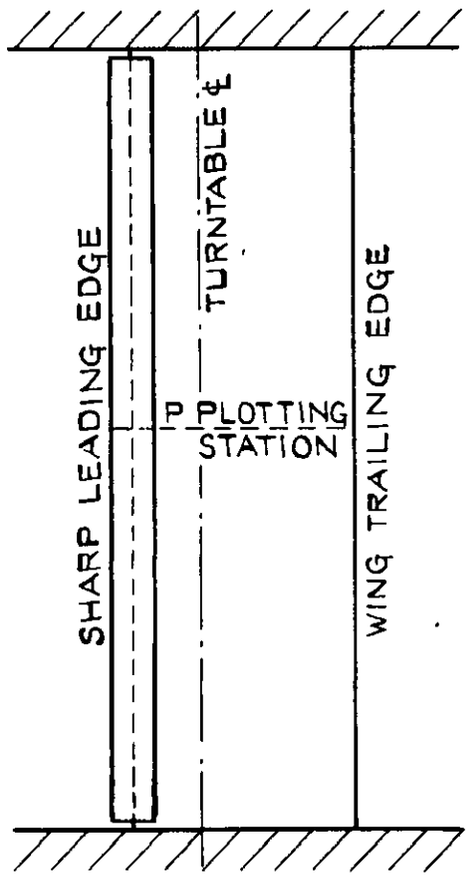

(d) SHARP LEADING EDGE

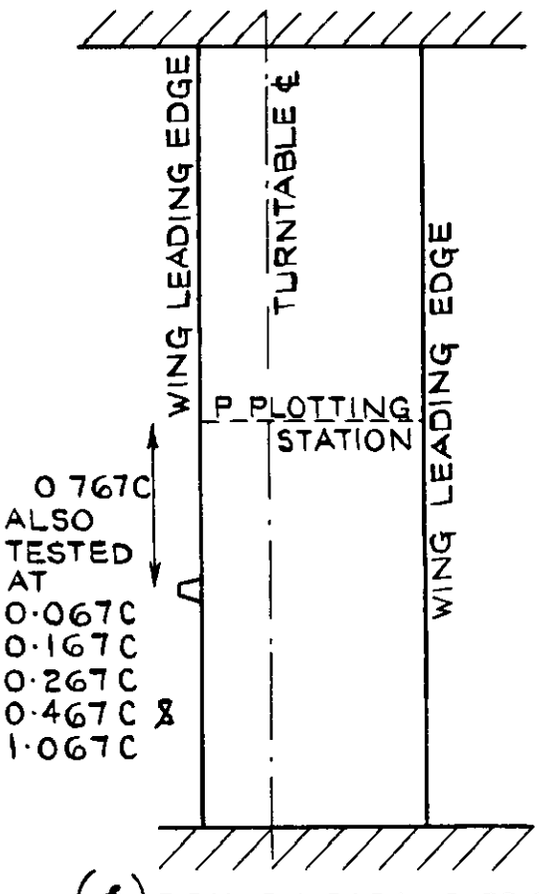

(f) ROUND LEADING EDGE – ISOLATED STRAKE

FIG. 1. MODEL DETAILS – PLANFORM VIEWS.

0 10 20 30

(a) ROUND LEADING EDGE
R.A.E. 101 SECTION 6% t/c

(b), (c) ROUND LEADING EDGE-STRAKES ON

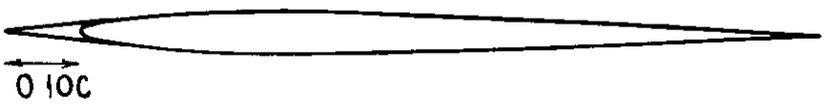

(d) SHARP LEADING EDGE

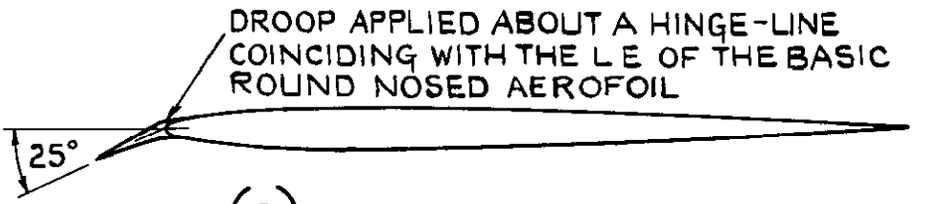

(e) SHARP LEADING EDGE
-NOSE FLAP DEFLECTED 25°

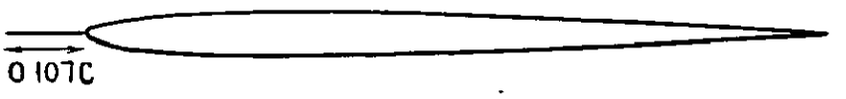

(f) ROUND LEADING EDGE
-ISOLATED STRAKE

FIG·2. MODEL DETAILS-WING SECTIONS.

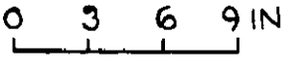

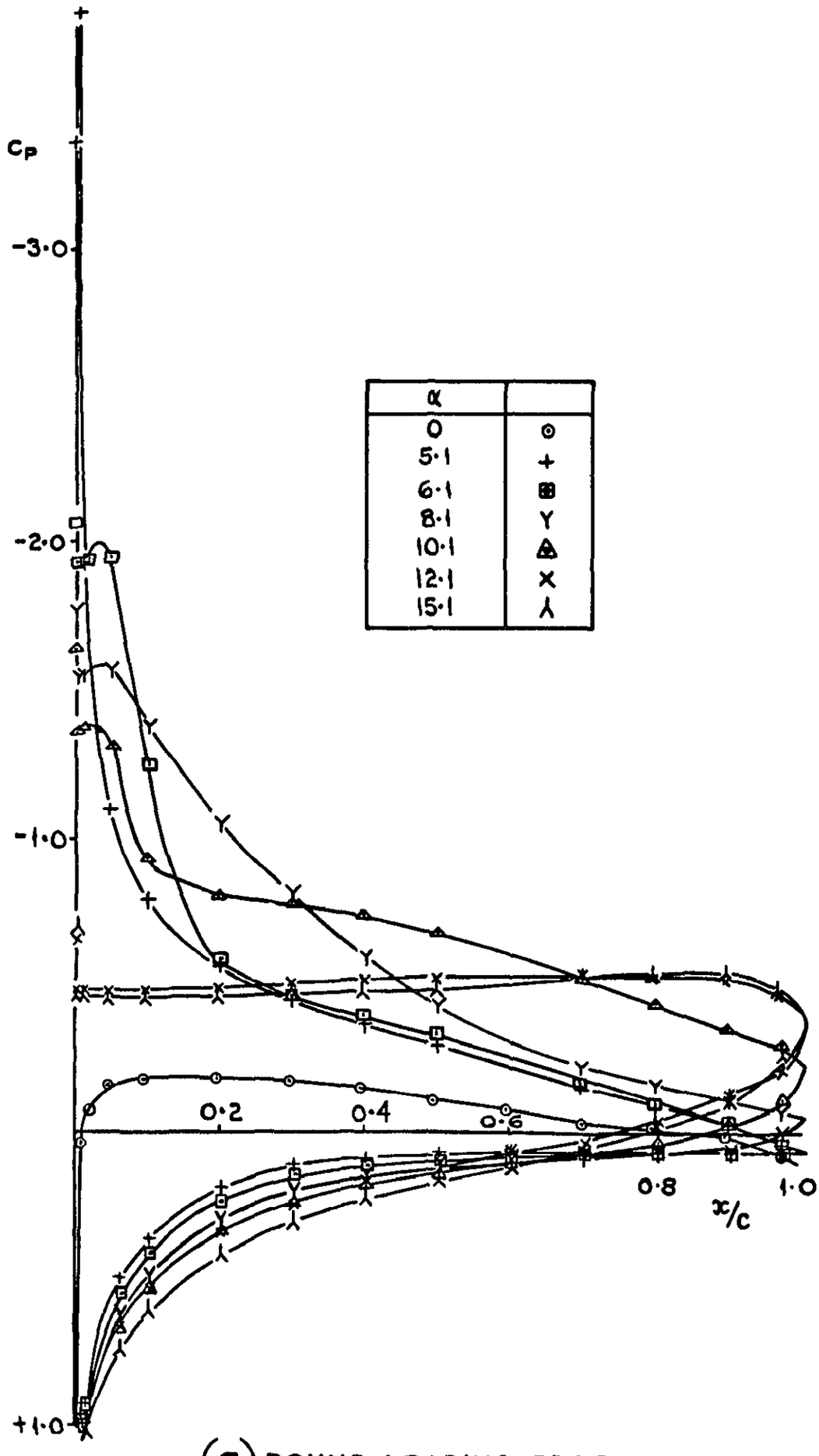

(a) ROUND LEADING EDGE

FIG. 3. SURFACE PRESSURE DISTRIBUTIONS.

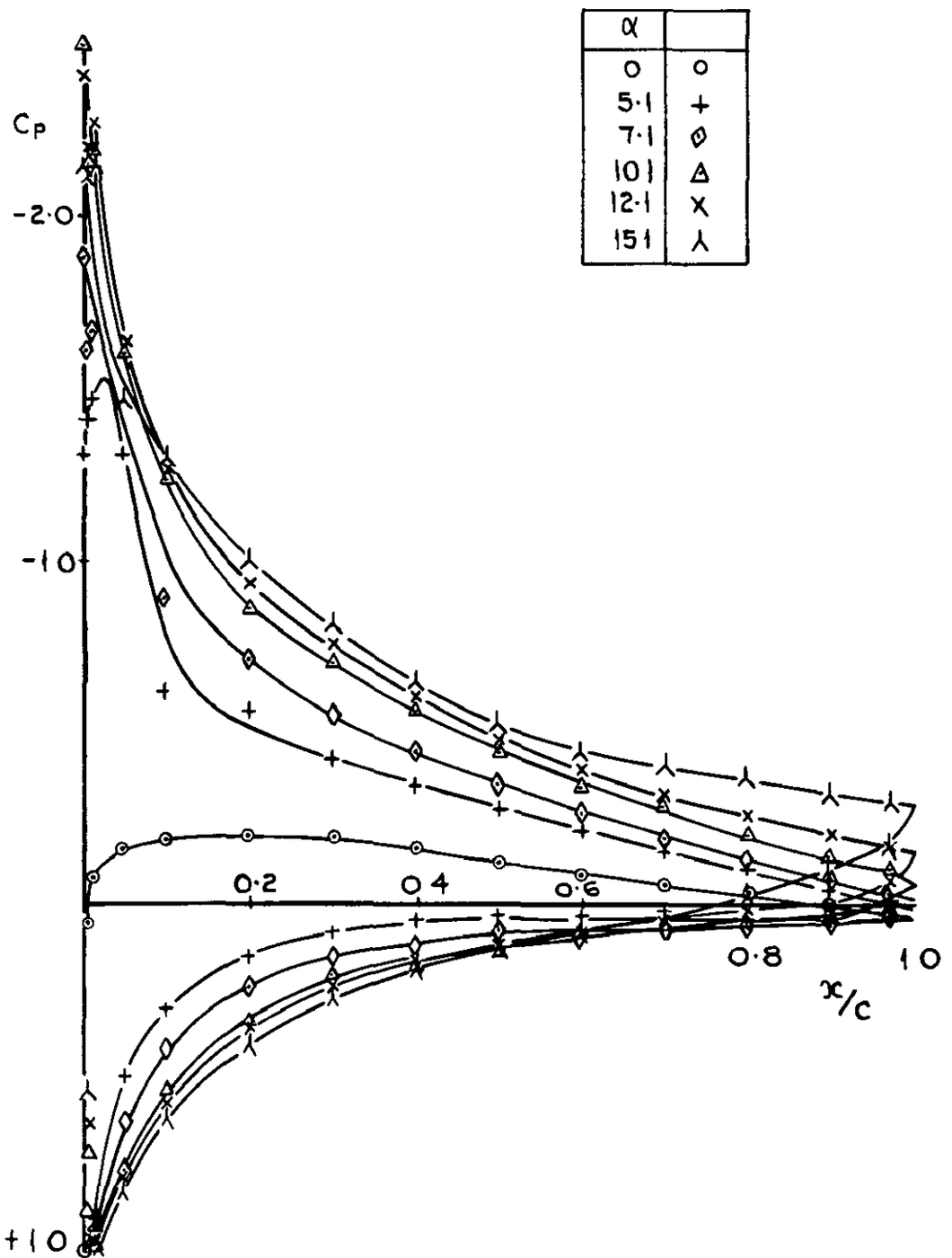

(b) ROUND LEADING EDGE – MIDWAY BETWEEN STRAKES

FIG. 3. (Cont)

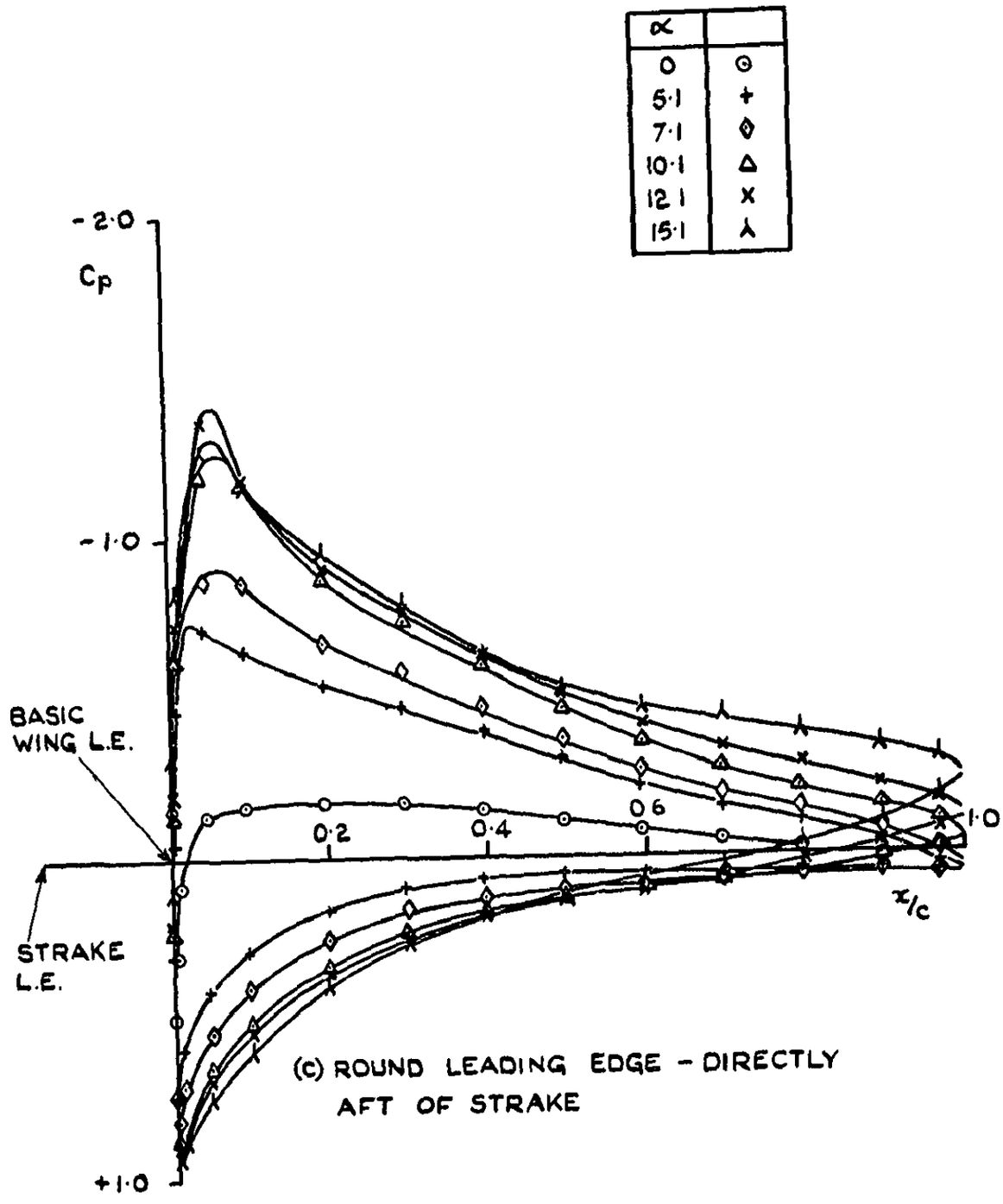
α
0
5·1
7·1
10·1
12·1
15·1
-2·0
Cp
-1·0
BASIC WING L.E.
STRAKE L.E.
0·2
0·4
0·6
1·0
x/c
+1·0
(c) ROUND LEADING EDGE - DIRECTLY AFT OF STRAKE

FIG. 3. (Cont)

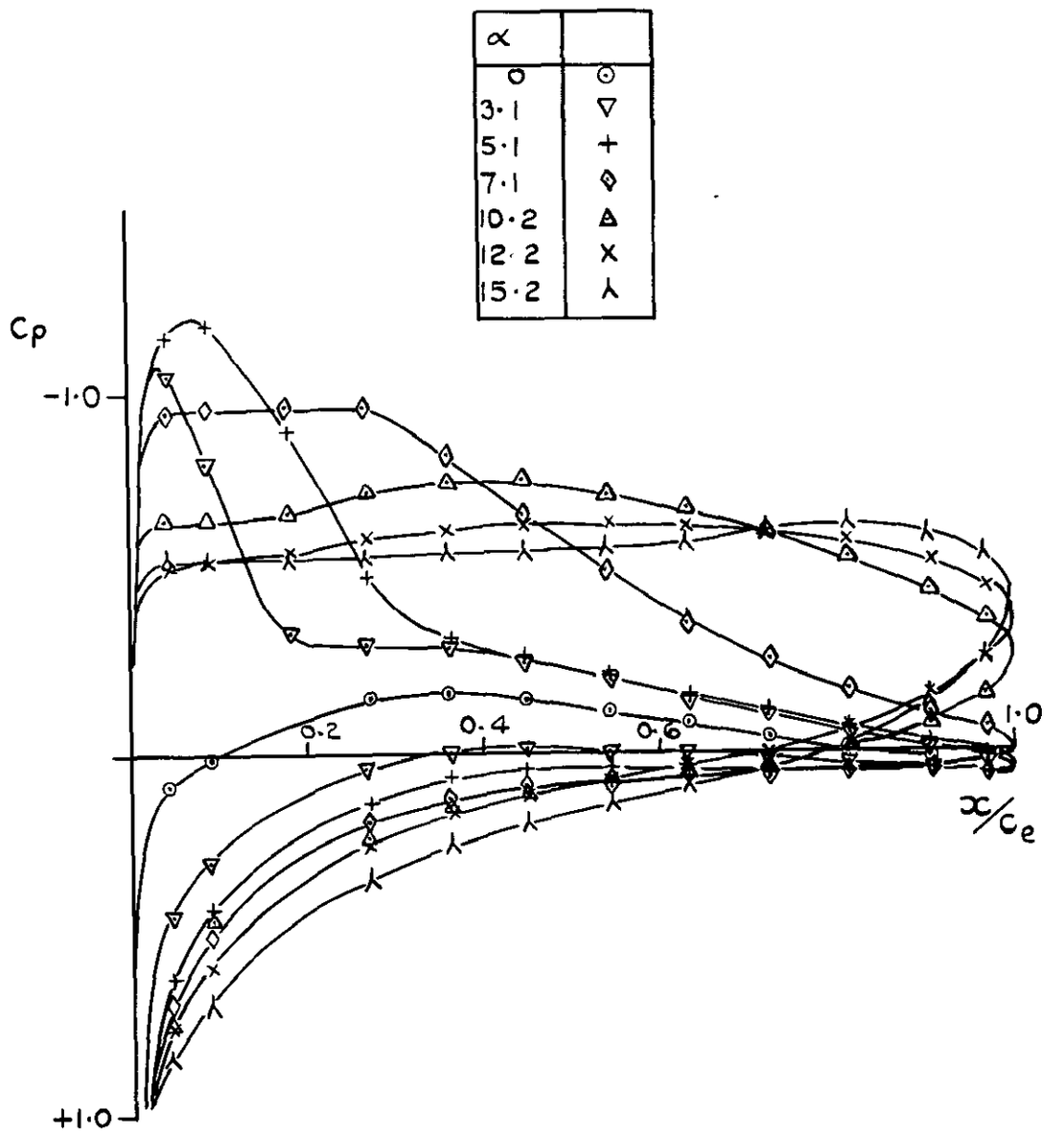

(d) SHARP LEADING EDGE
$\left(\frac{x}{c_e}\right.$ BASED ON EXTENDED CHORD$\left.\right)$

FIG. 3. (Cont)

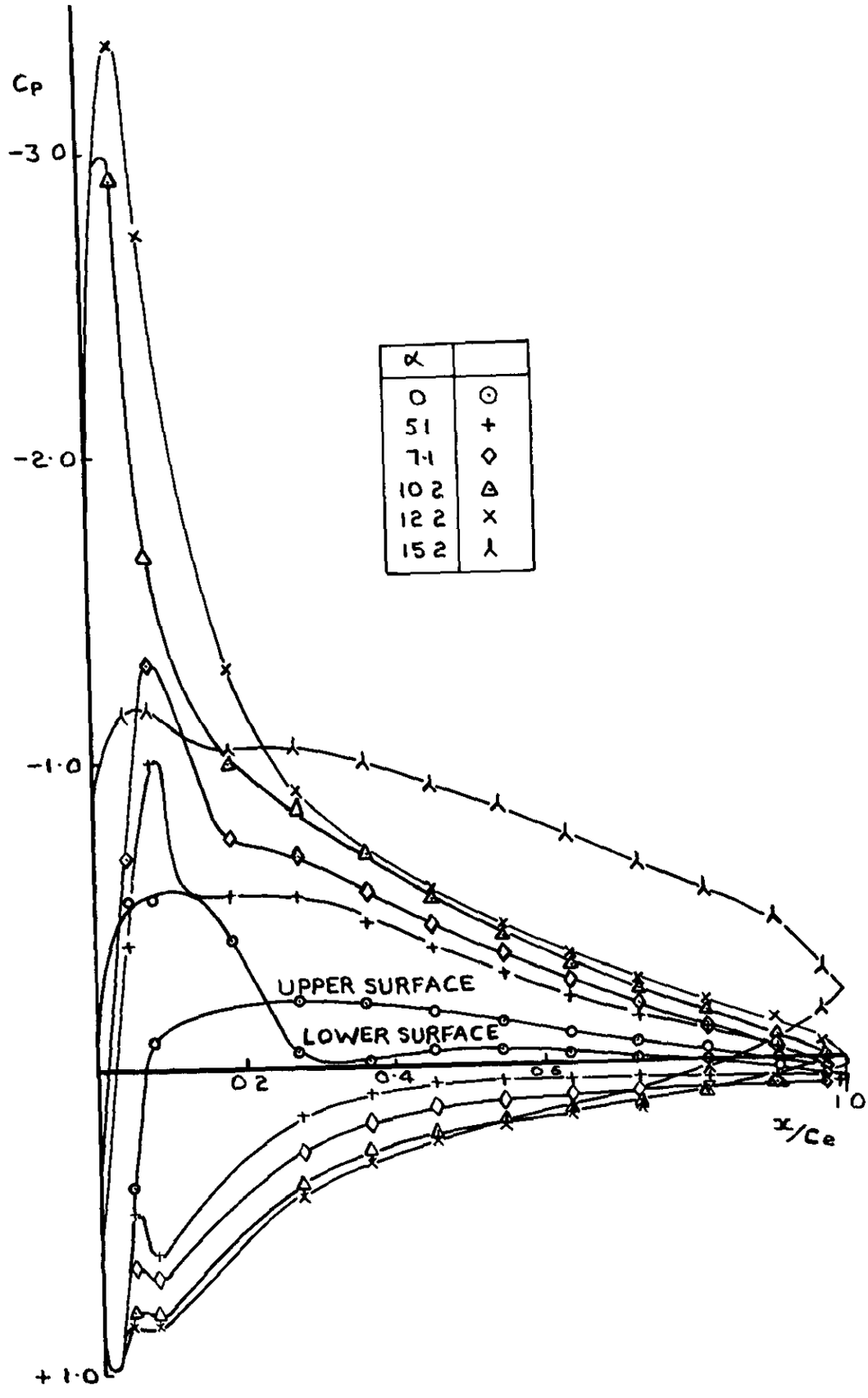

(e) SHARP LEADING EDGE-NOSE FLAP DEFLECTED 25°
($\frac{x}{c_e}$ BASED ON EXTENDED CHORD)

FIG. 3. (Cont)

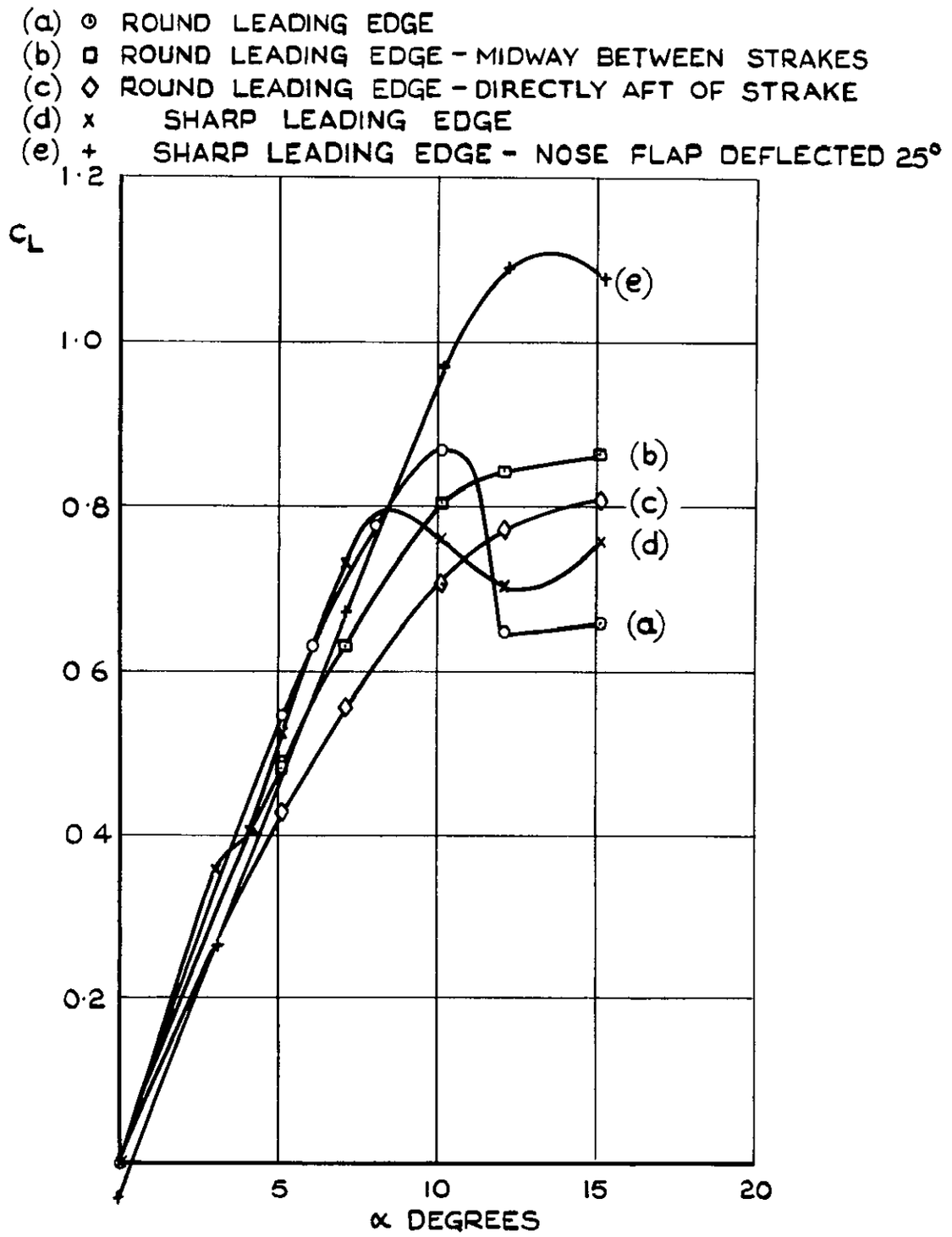

FIG. 4. LIFT COEFFICIENT VERSUS INCIDENCE.

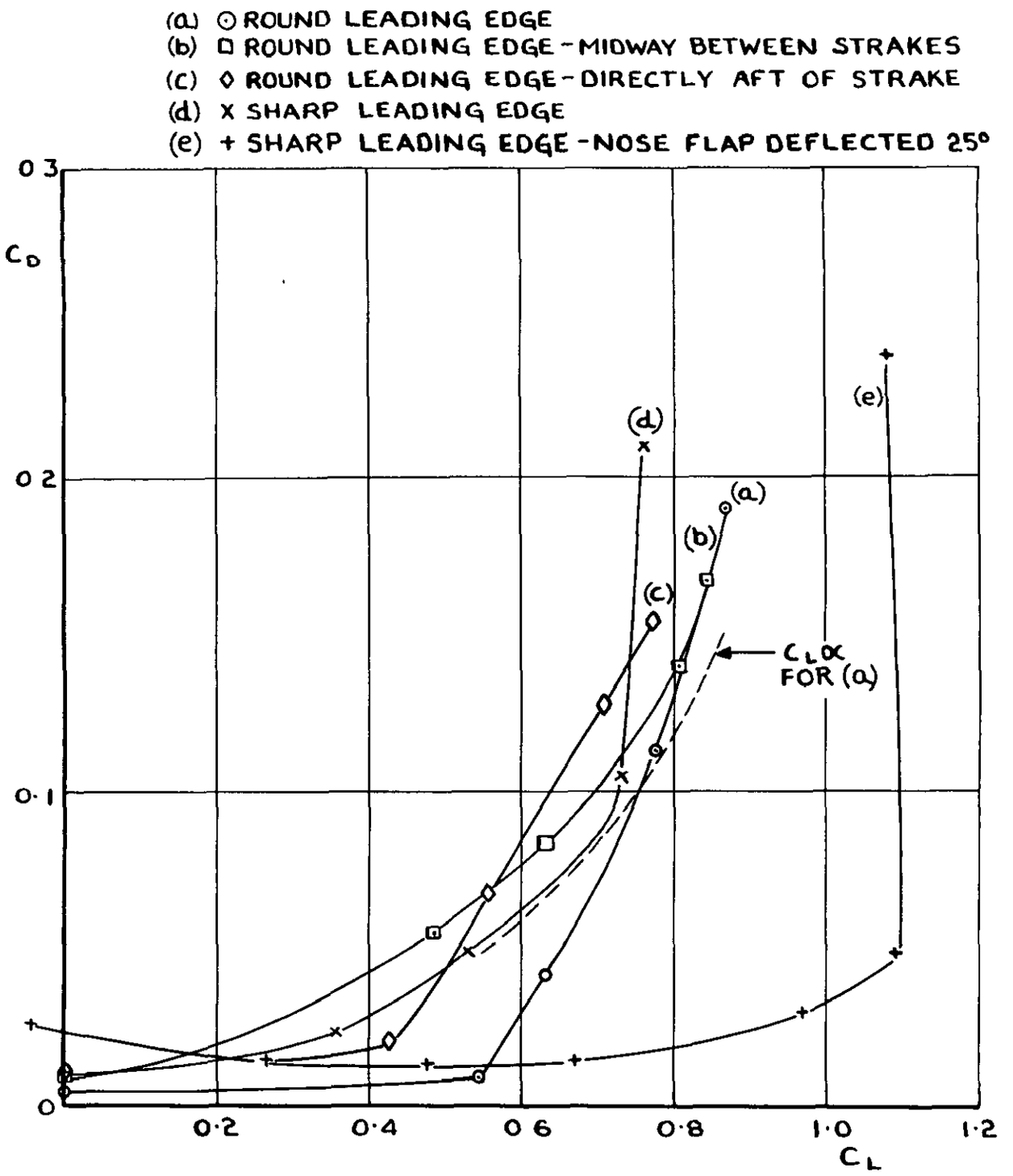

FIG. 5. DRAG COEFFICIENT VERSUS LIFT COEFFICIENT.

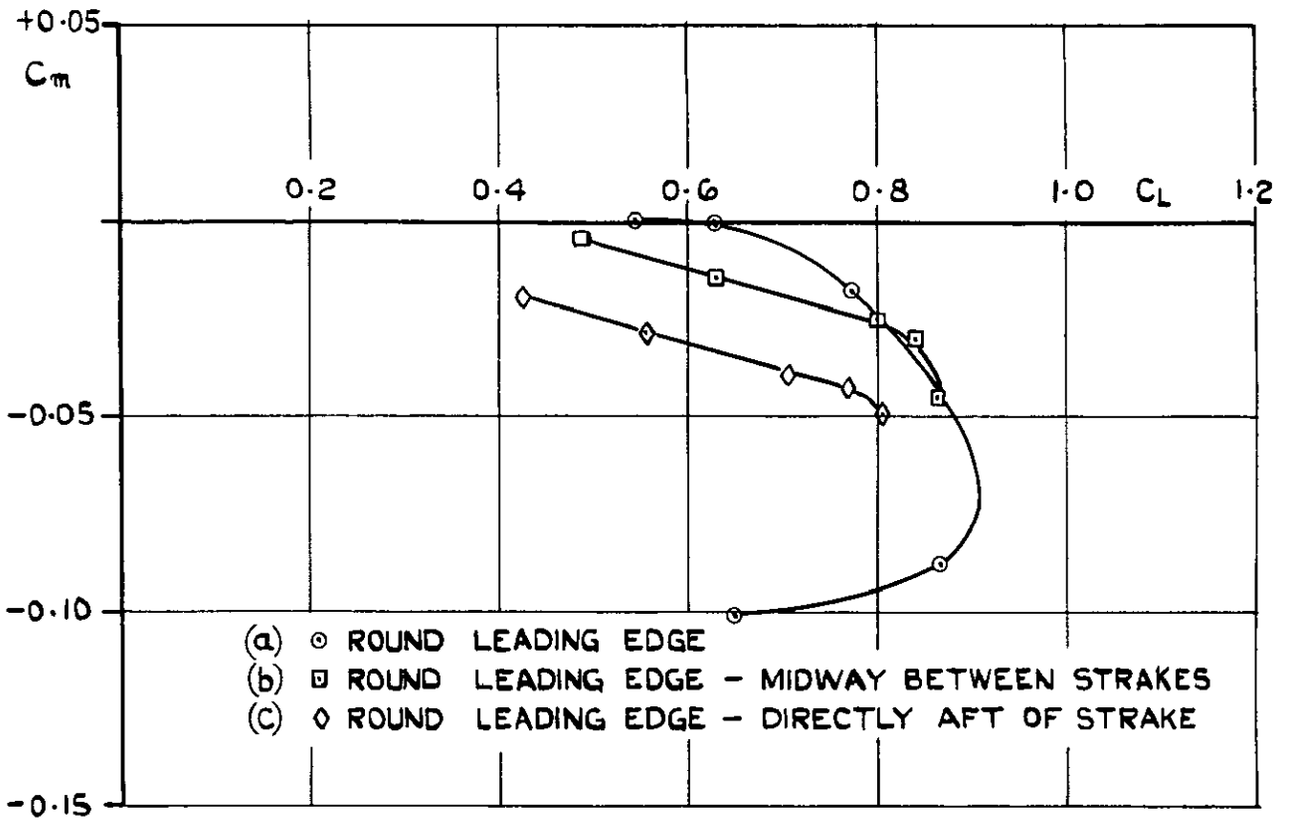

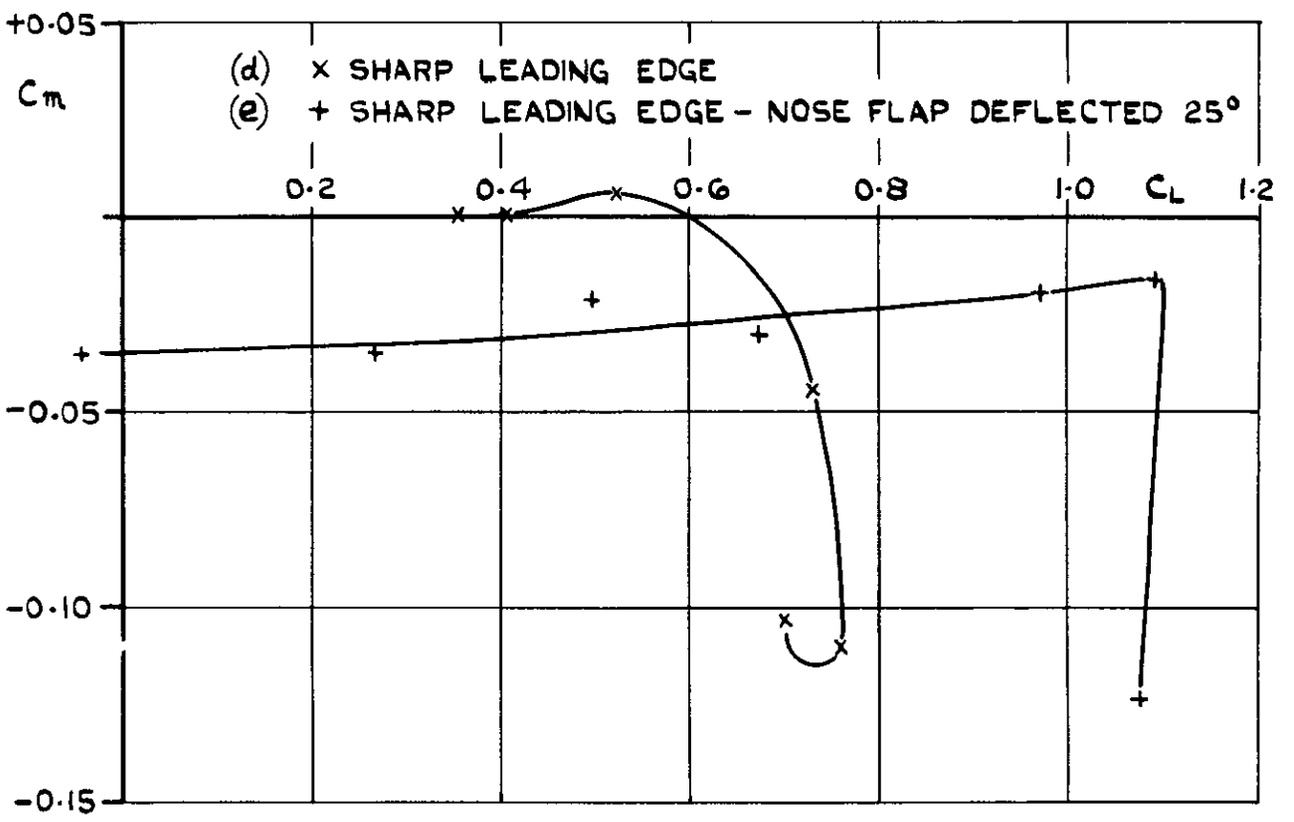

FIG. 6. PITCHING MOMENT COEFFICIENT VERSUS LIFT COEFFICIENT.

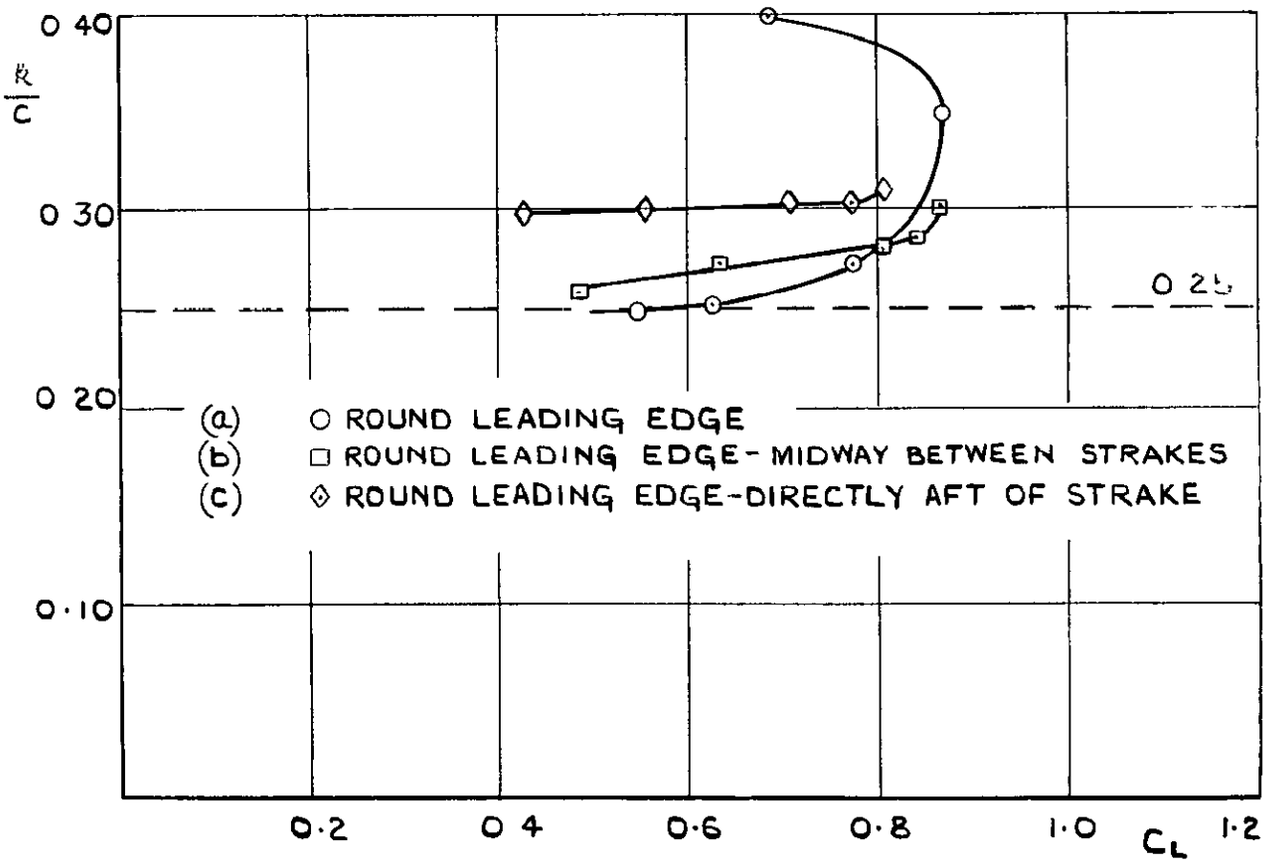

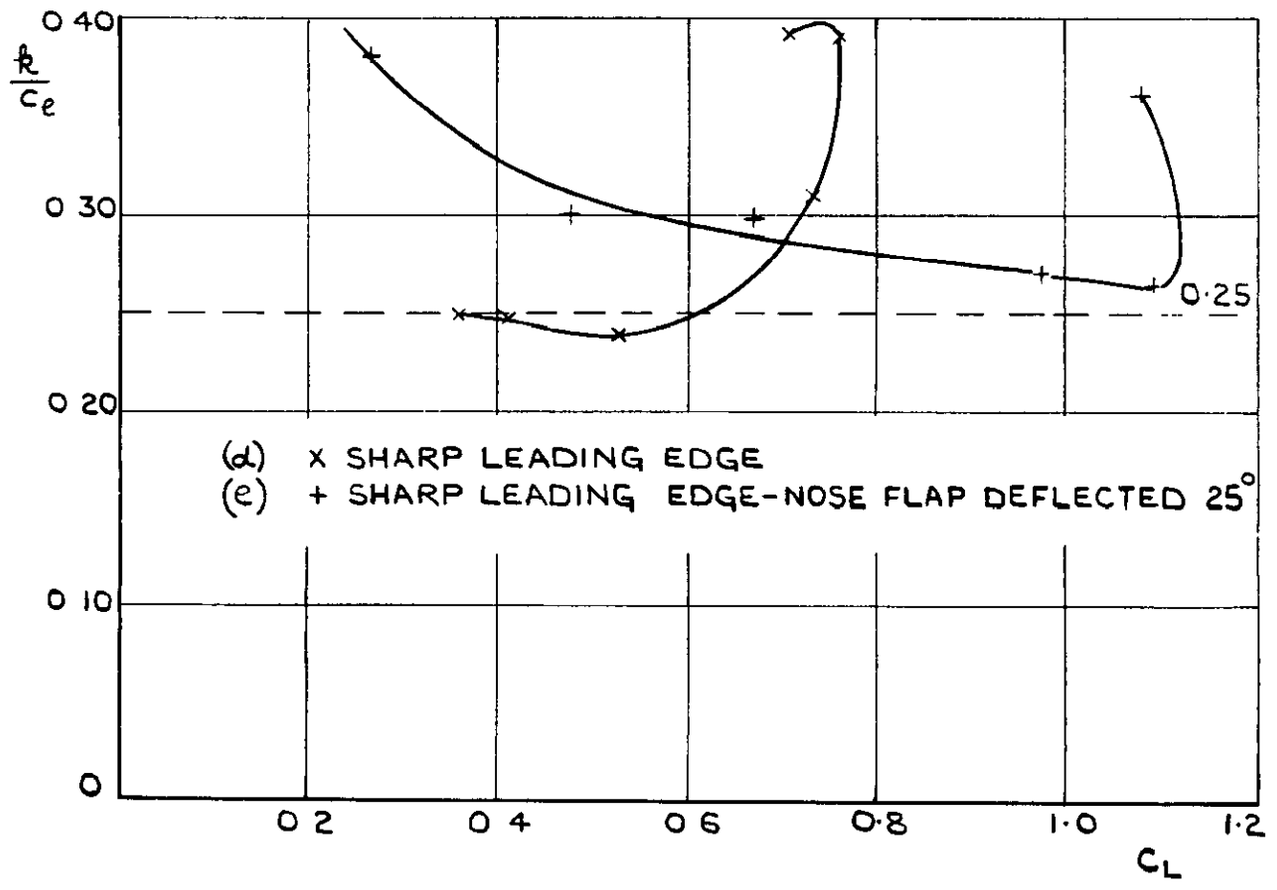

FIG .7. CENTRE OF PRESSURE POSITION VERSUS LIFT COEFFICIENT.

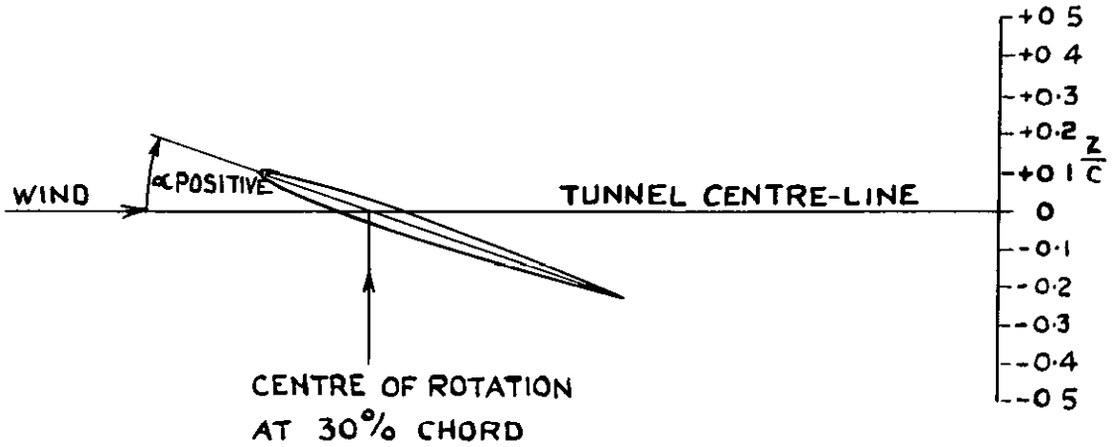

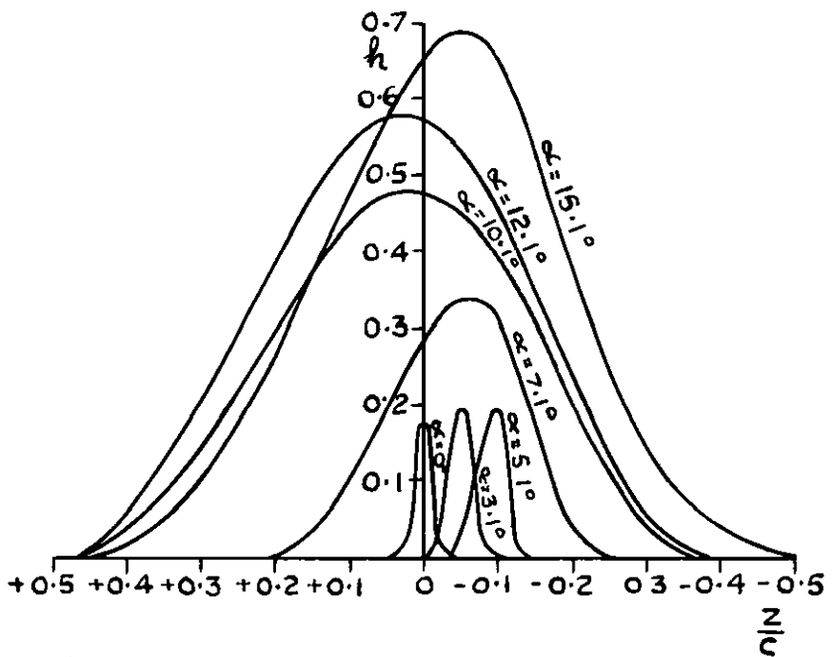

(a) ROUND LEADING EDGE

WAKE TRAVERSES 1·0C
BEHIND WING TRAILING EDGE

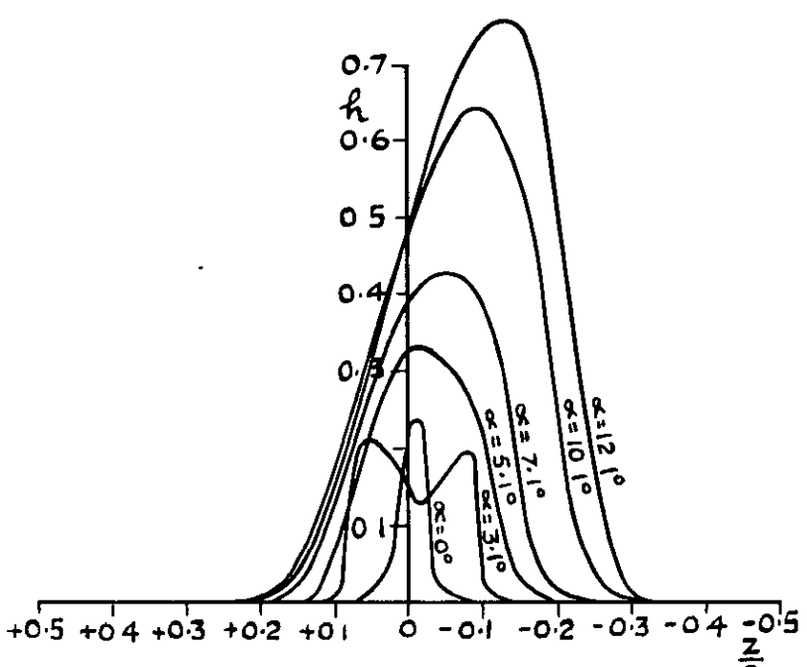

(b) ROUND LEADING EDGE
MIDWAY BETWEEN STRAKES

WAKE TRAVERSES 1·0C BEHIND
WING TRAILING EDGE

FIG. 8. WAKE TRAVERSES.

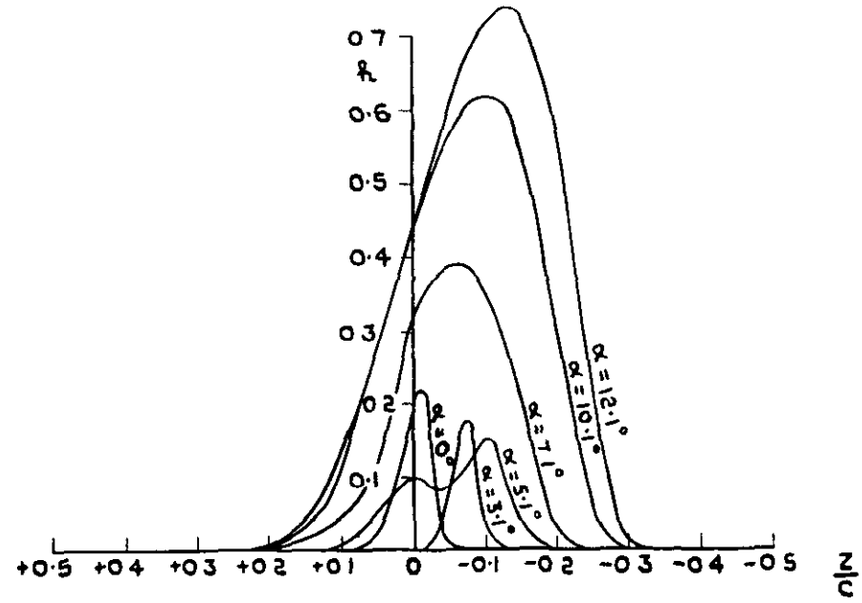

(c) ROUND LEADING EDGE – DIRECTLY AFT OF STRAKE
WAKE TRAVERSES 1·0C BEHIND WING TRAILING EDGE

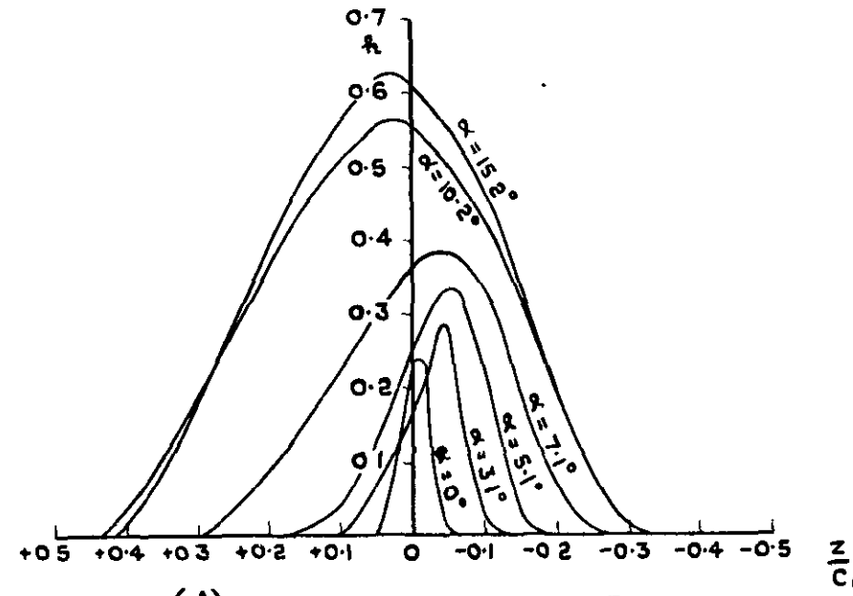

(d) SHARP LEADING EDGE
WAKE TRAVERSES 0·9C_e BEHIND WING TRAILING EDGE

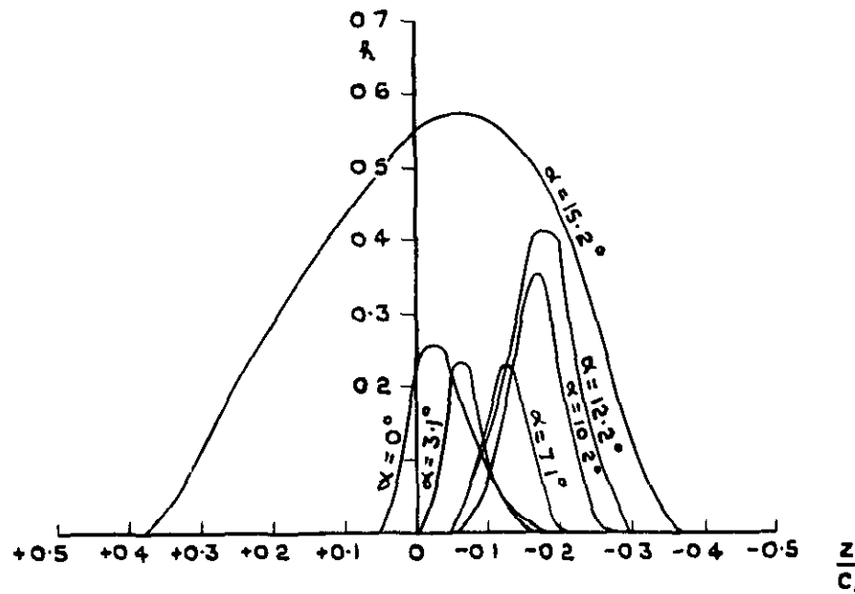

(e) SHARP LEADING EDGE – NOSE FLAP DEFLECTED 25°
WAKE TRAVERSES 0·9C_e BEHIND WING TRAILING EDGE

FIG. 8. (Cont)

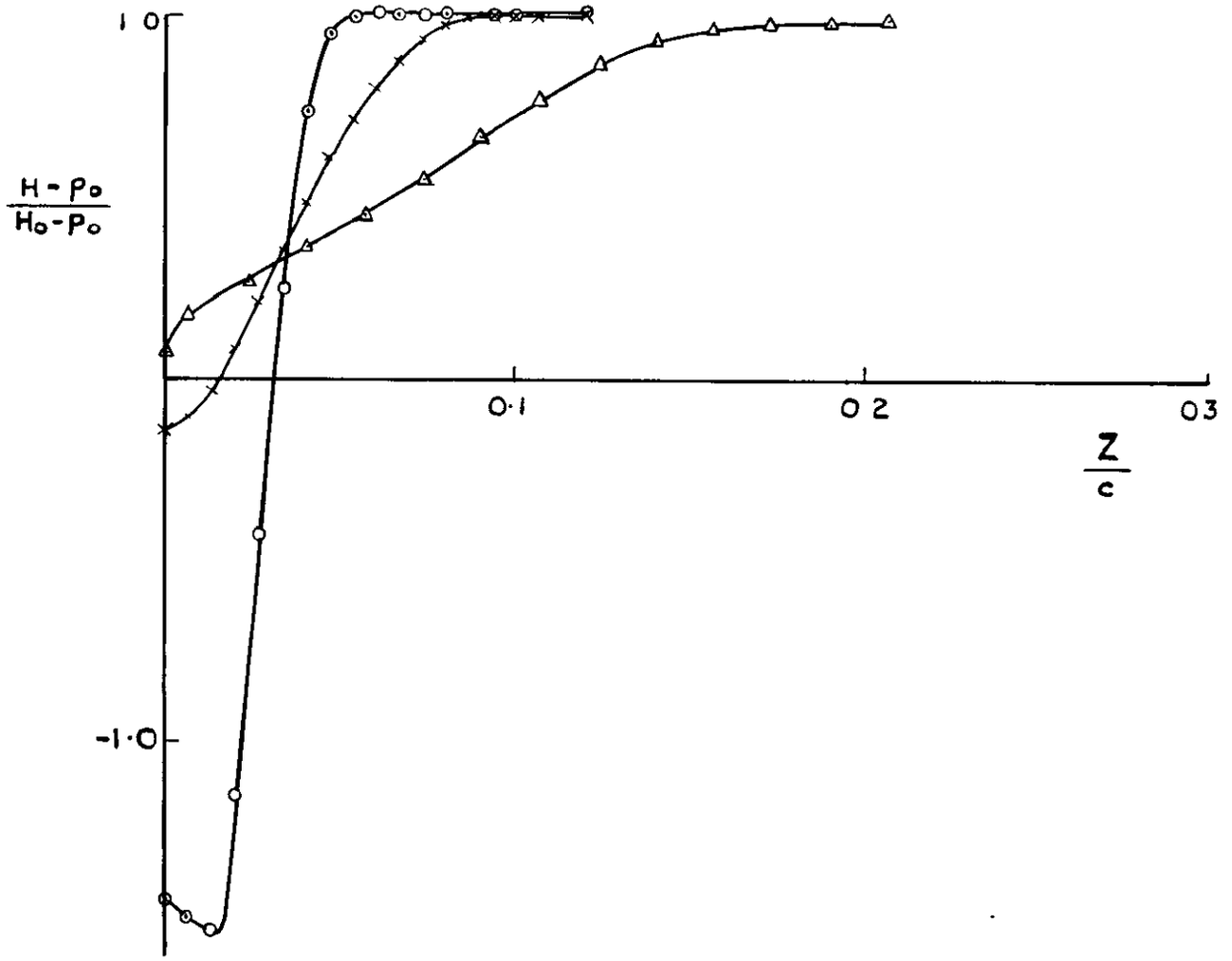

$\alpha = 7.1^\circ$ (UPPER SURFACE)

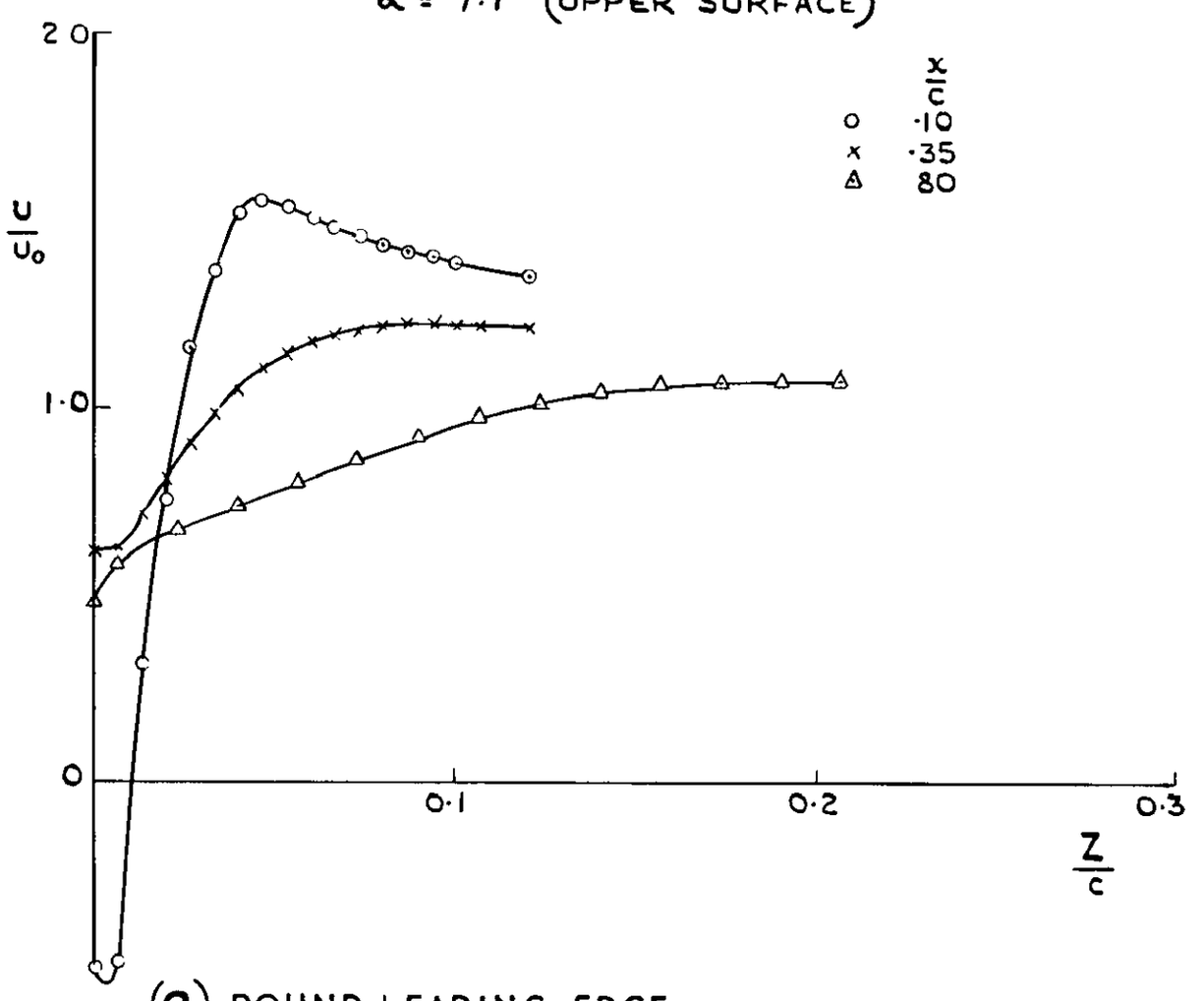

(a) ROUND LEADING EDGE

FIG.9. TOTAL HEAD & VELOCITY TRAVERSES.

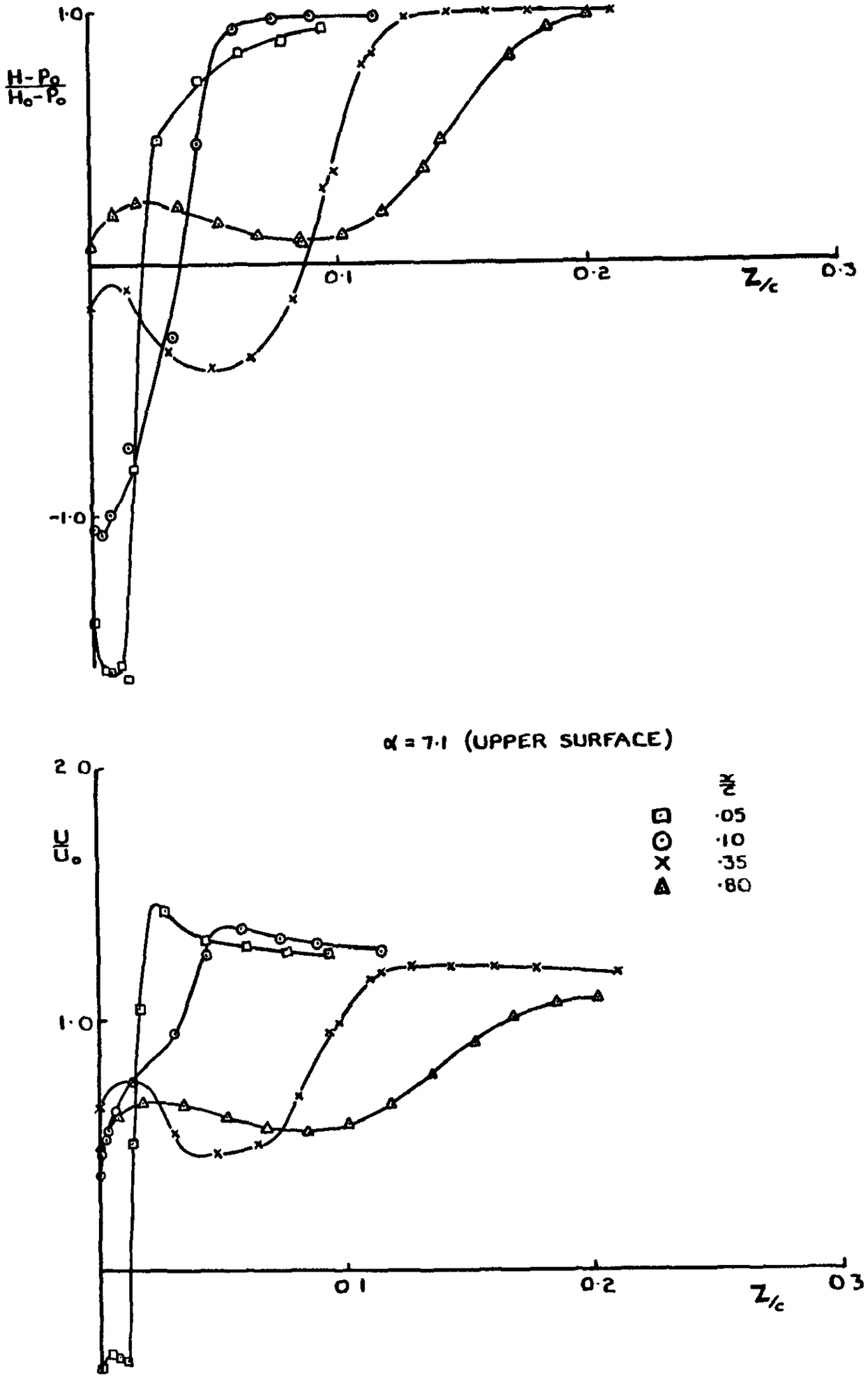

(b) ROUND LEADING EDGE — MIDWAY BETWEEN STRAKES

FIG. 9. (Cont)

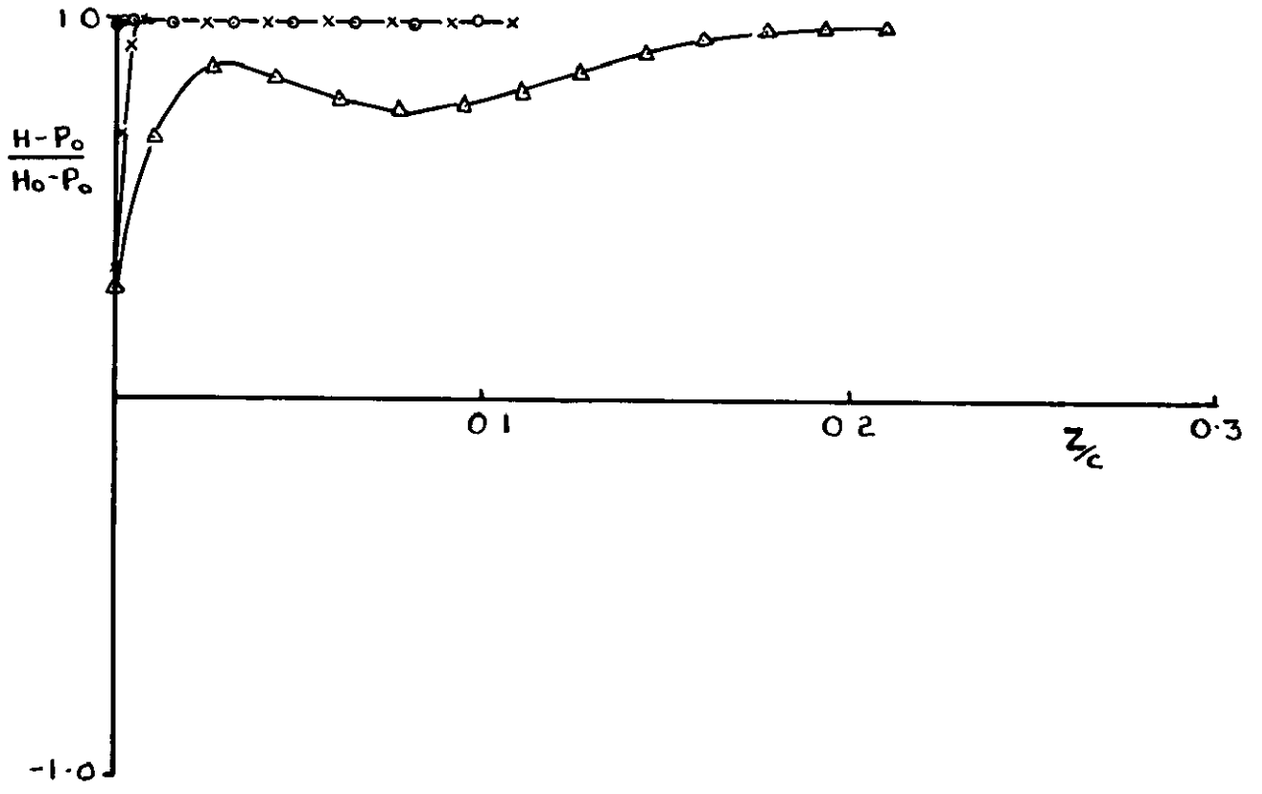

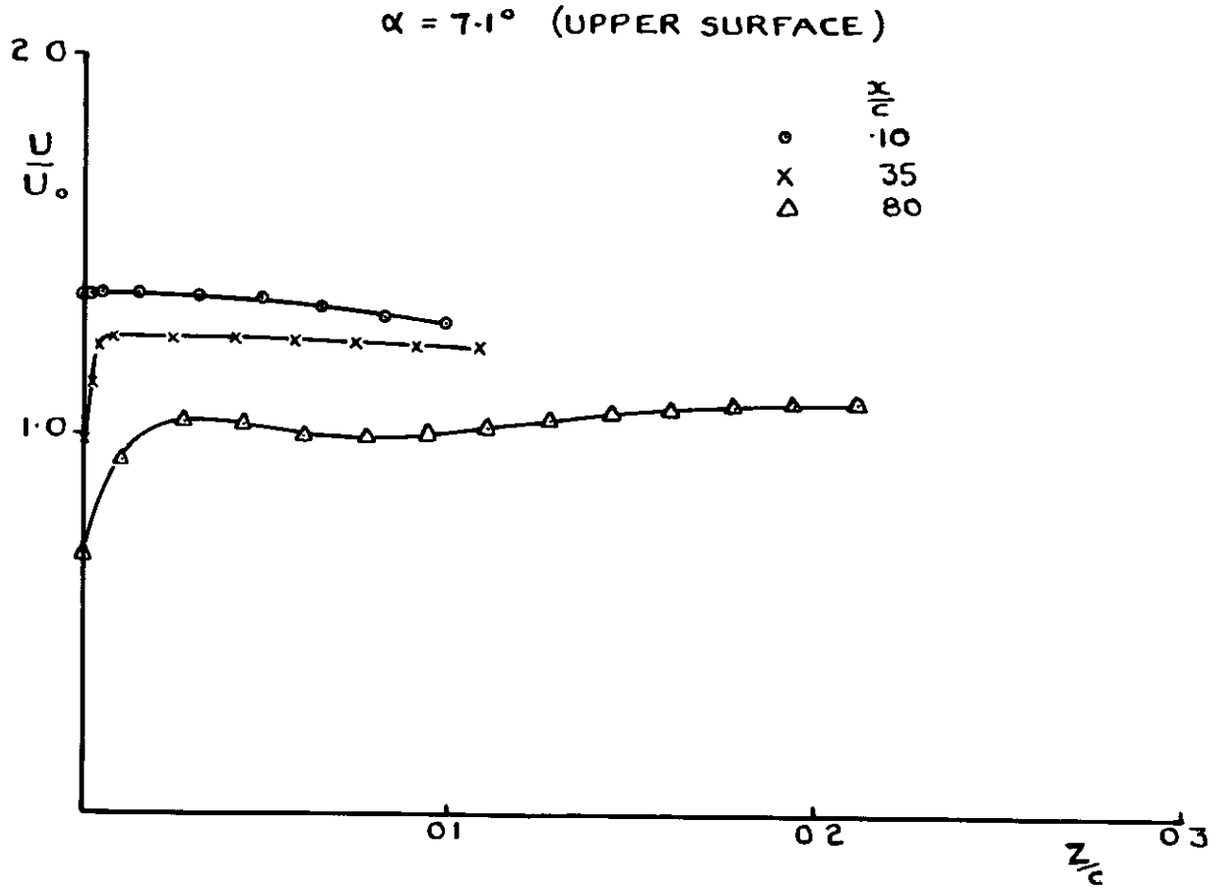

(C) ROUND LEADING EDGE – DIRECTLY AFT OF STRAKE

FIG. 9. (Cont)

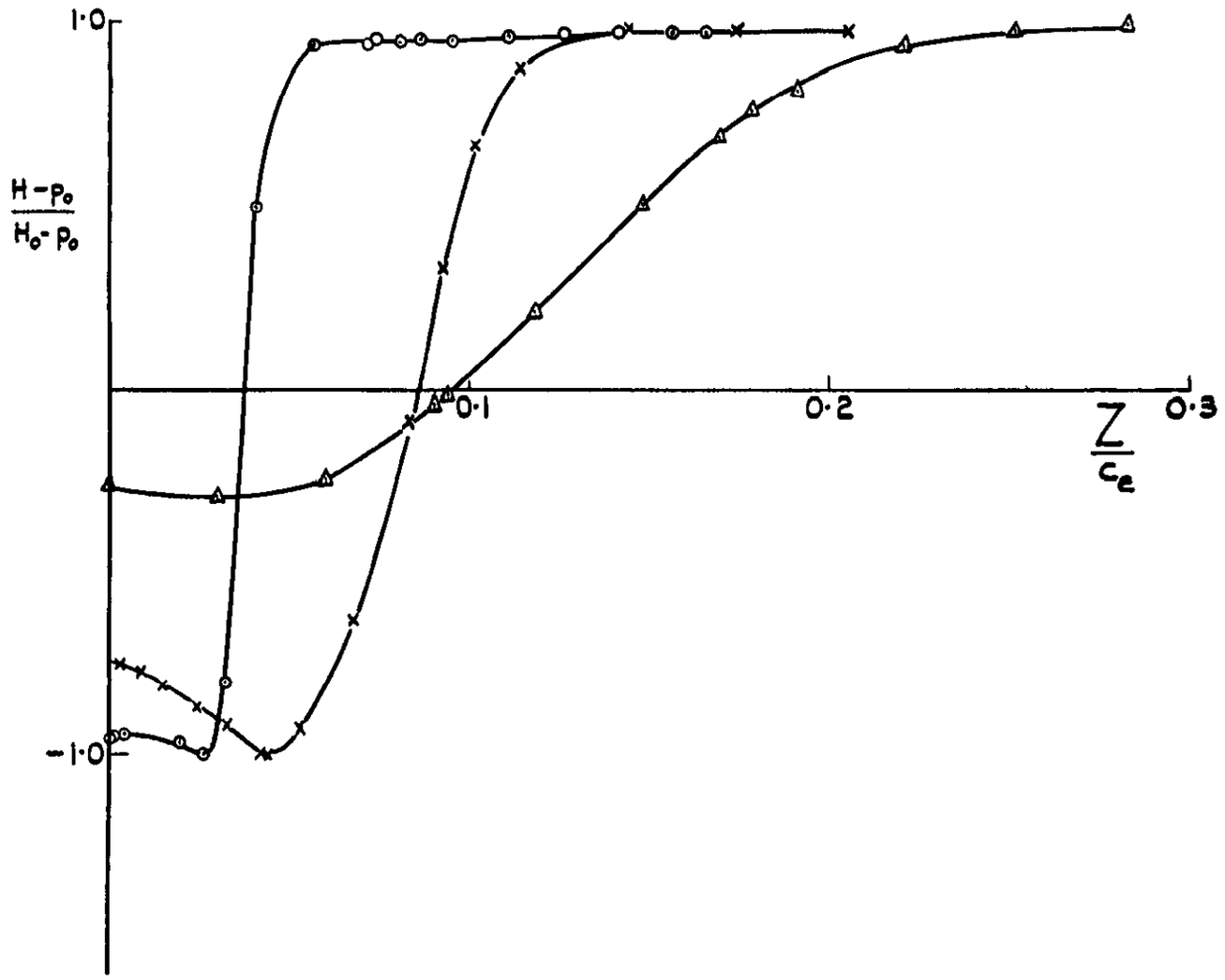

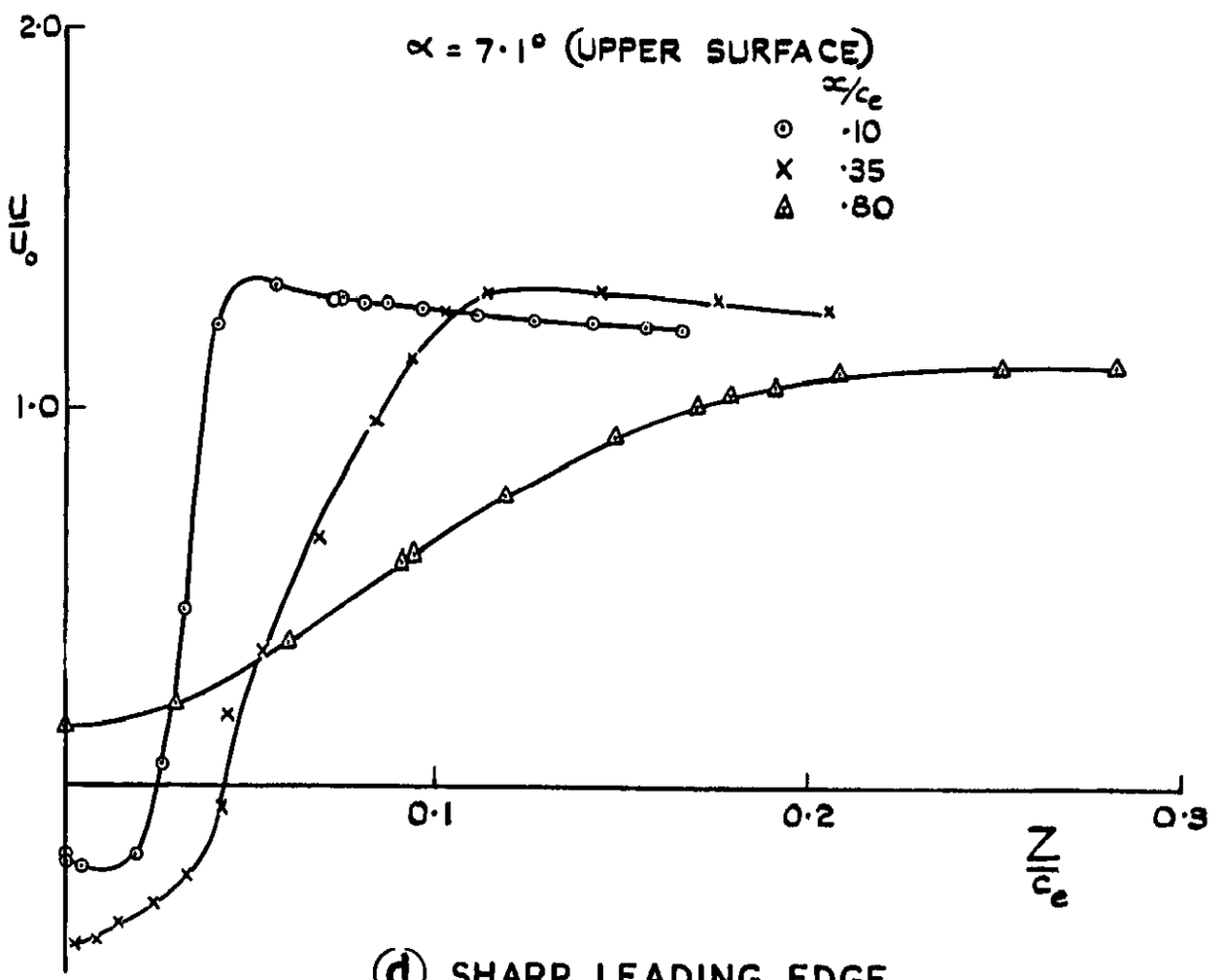

(d) SHARP LEADING EDGE

FIG. 9. (Cont)

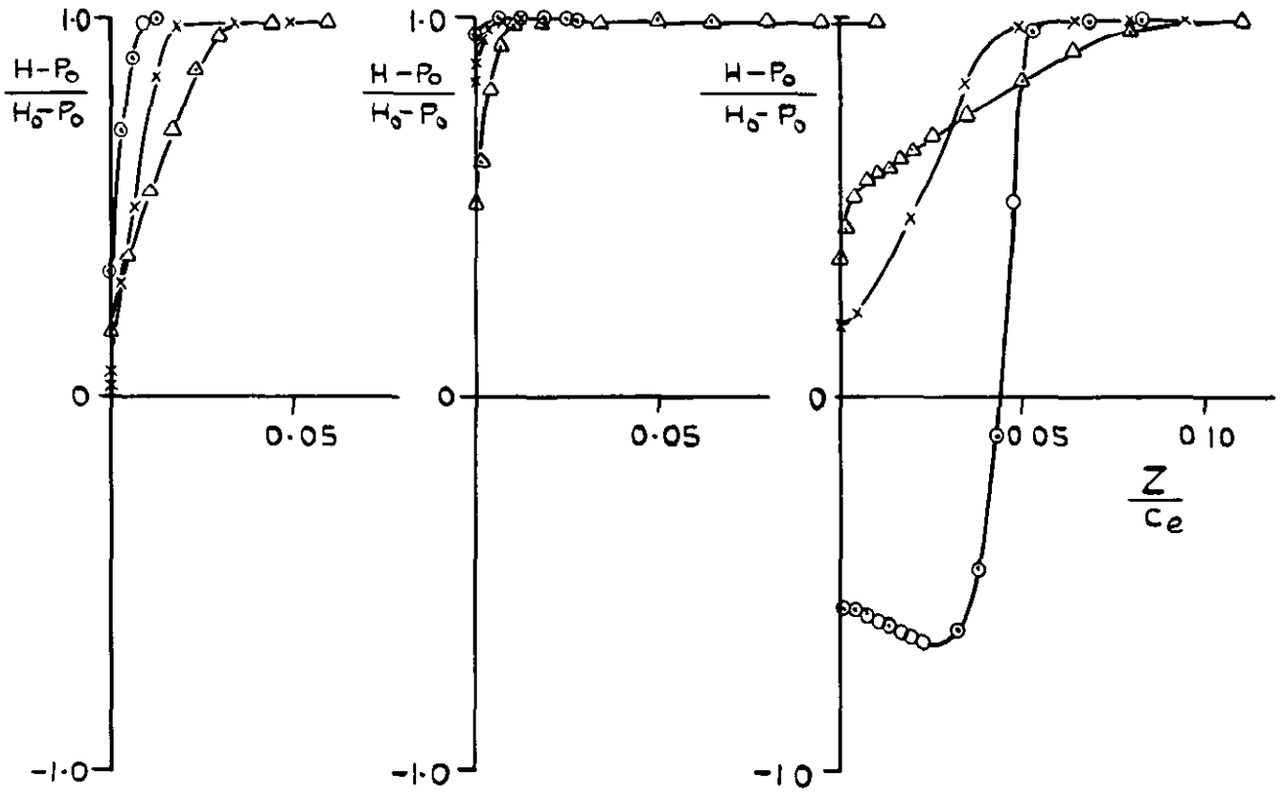

α = 7·1° (UPPER SURFACE) α = 7·1° (LOWER SURFACE) α = 0° (LOWER SURFACE)

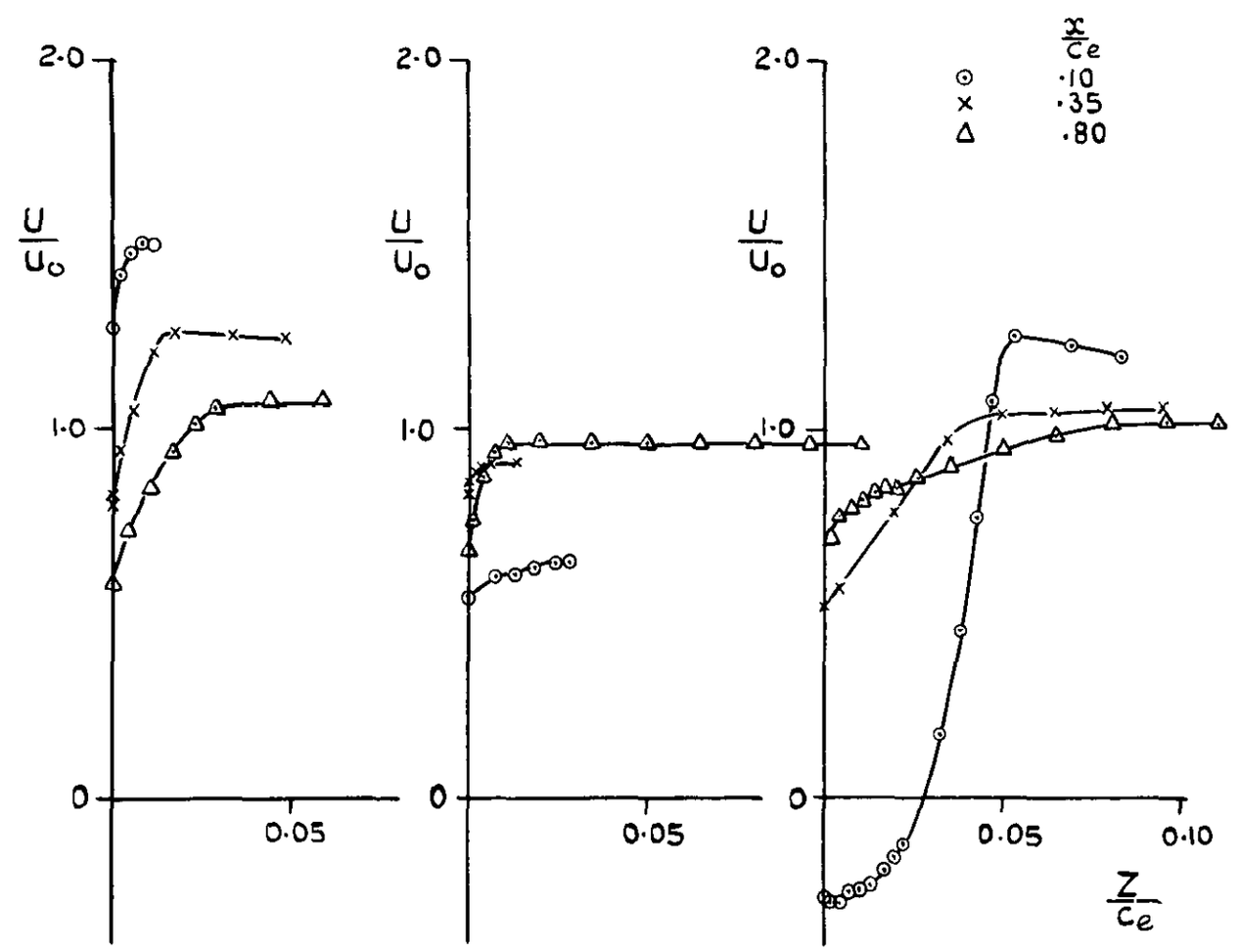

(e) SHARP LEADING EDGE-NOSE FLAP DEFLECTED 25°

FIG. 9. (Cont)

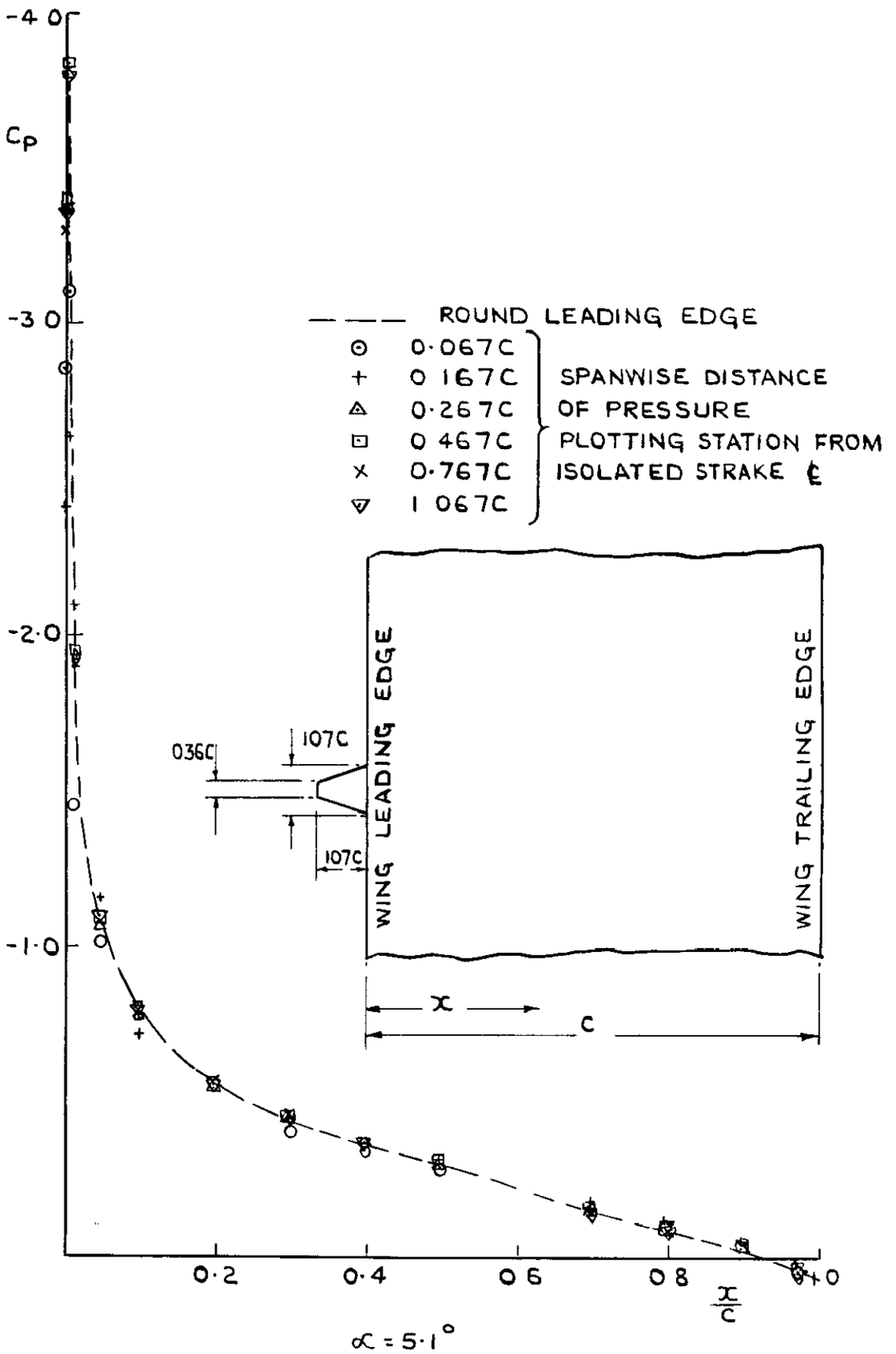

FIG. 10. UPPER SURFACE PRESSURE DISTRIBUTIONS AT VARIOUS SPANWISE DISTANCES FROM AN ISOLATED STRAKE.

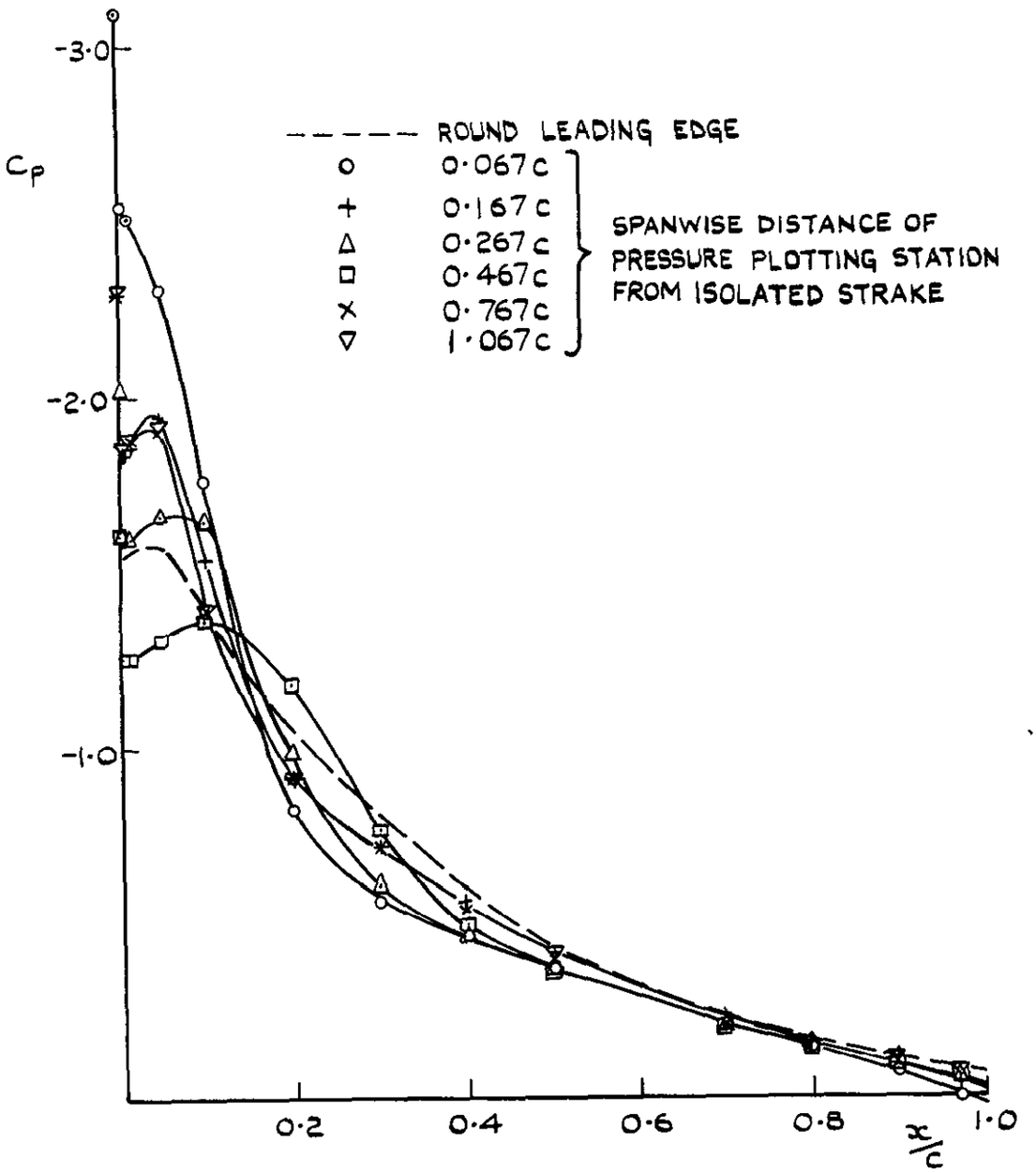

$\alpha = 8{\cdot}1^{\circ}$

FIG. 10. (Cont)

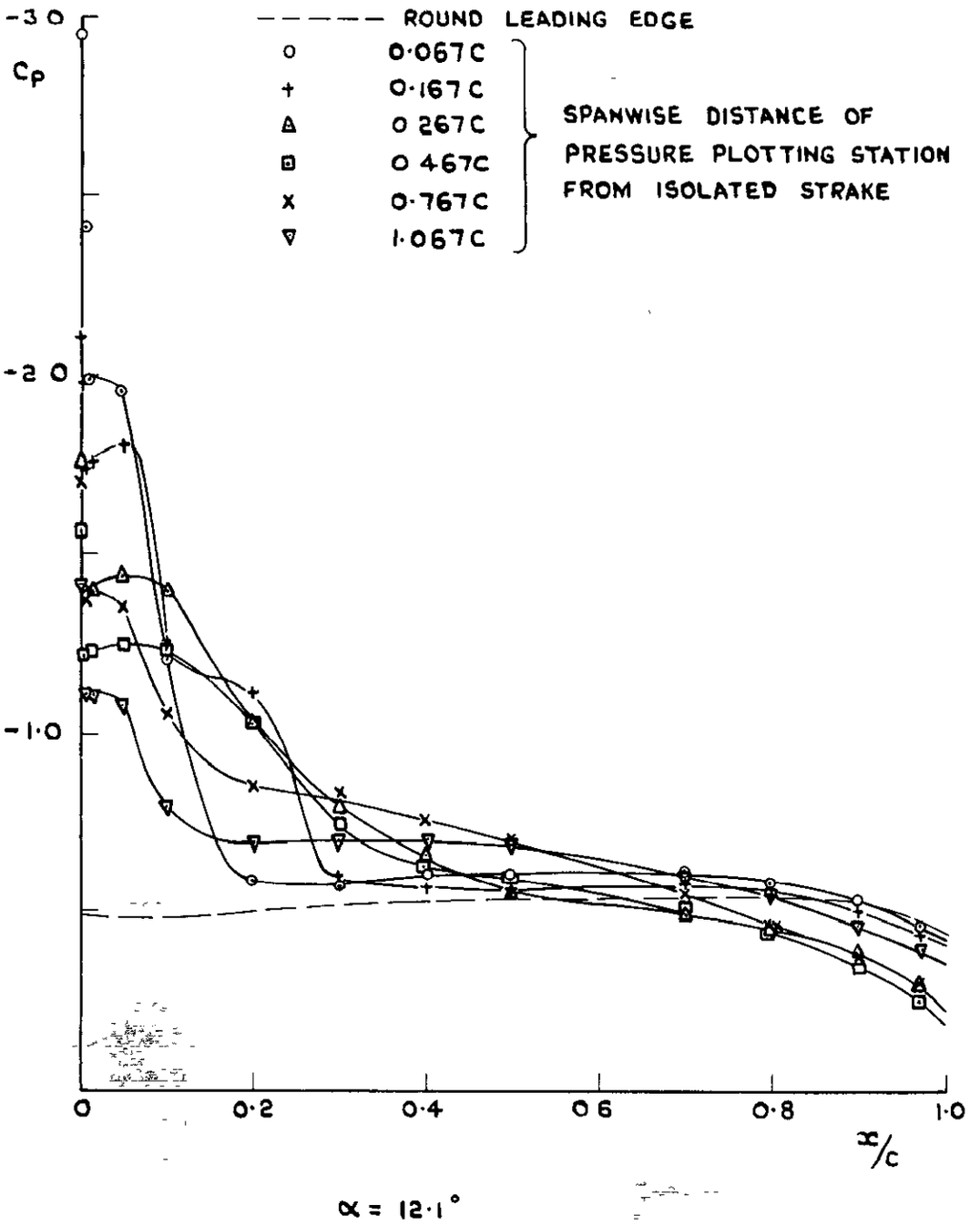
-3 0
C_p
-2 0
-1·0
0
0·2
0·4
0 6
0·8
1·0
x/c
ROUND LEADING EDGE
0·067C
0·167 C
0 267C
0 467C
0·767C
1·067C
SPANWISE DISTANCE OF PRESSURE PLOTTING STATION FROM ISOLATED STRAKE
α = 12·1°

FIG. 10. (Cont)

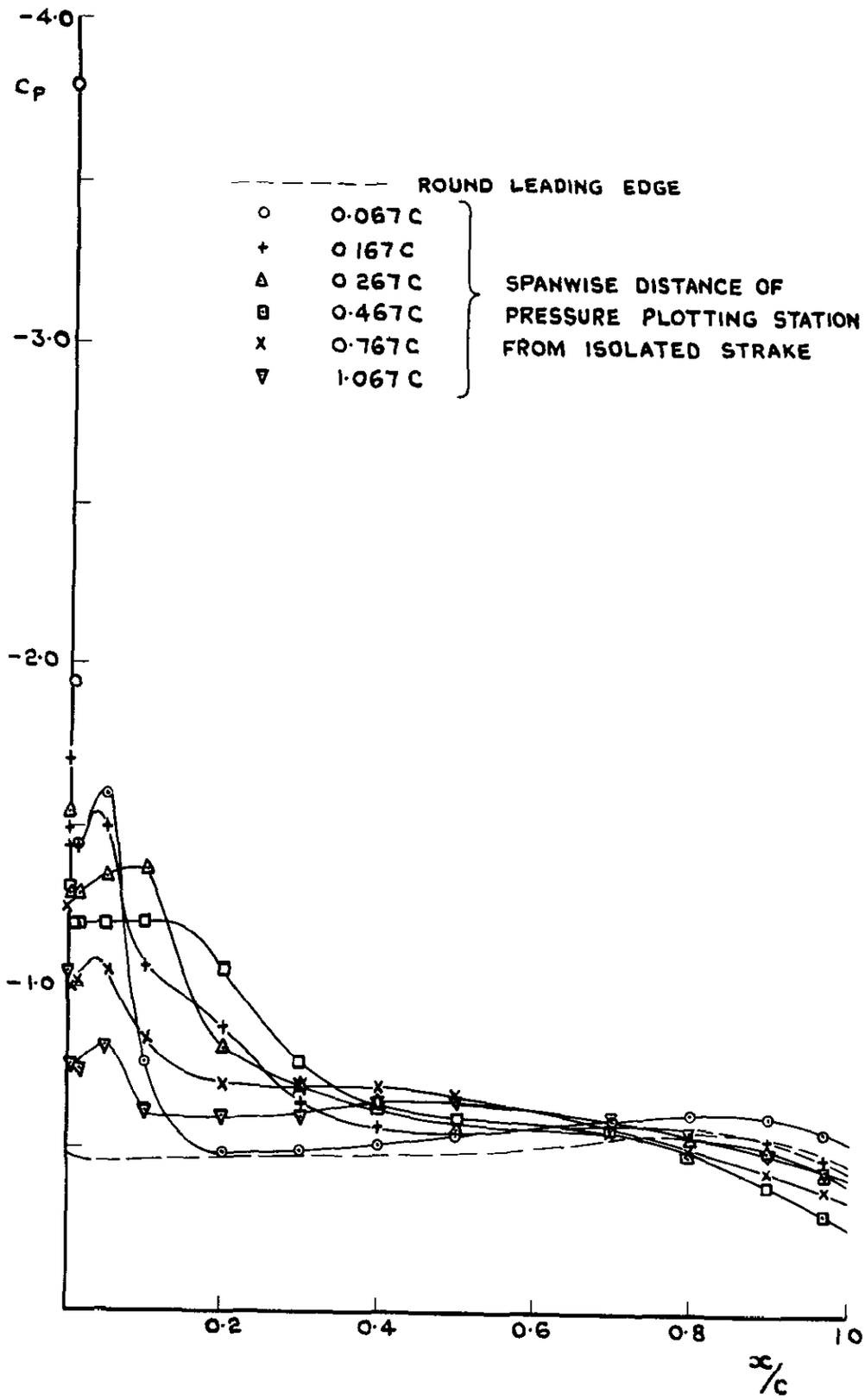
-4·0
C_P
-3·0
-2·0
-1·0
ROUND LEADING EDGE
0·067 C
0 167 C
0 267 C
0·467 C
0·767 C
1·067 C
SPANWISE DISTANCE OF PRESSURE PLOTTING STATION FROM ISOLATED STRAKE
0·2
0·4
0·6
0·8
1·0
x/c
α = 15·1°

FIG. 10. (Cont)

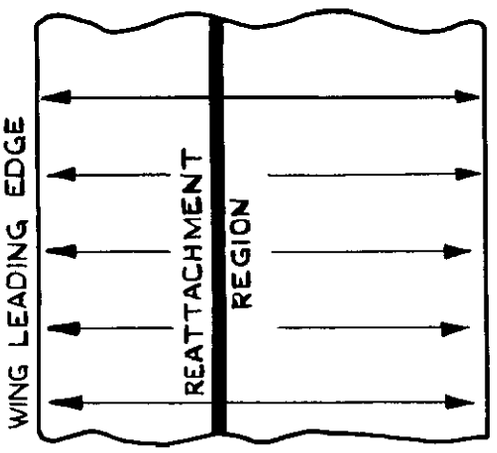

α	REATTACMENT POSITION
6·1°	12 – 15 % C
8·1°	35 – 45 % C
9·1°	80 – 100 % C
10·1°	NO REATTACHMENT

(a) ROUND LEADING EDGE
($\alpha = 8 \cdot 1°$)

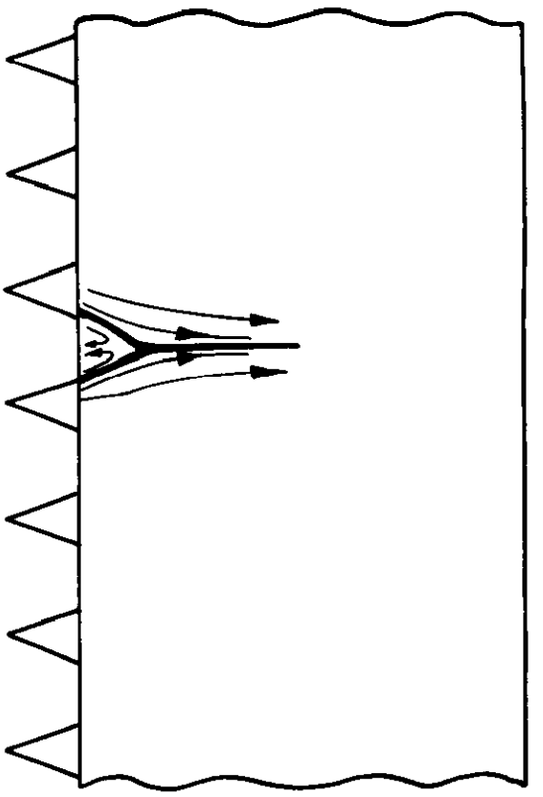

(b),(c) ROUND LEADING EDGE WITH ROW OF STRAKES
($\alpha = 7 \cdot 1°$ TO $\alpha = 15 \cdot 1°$)

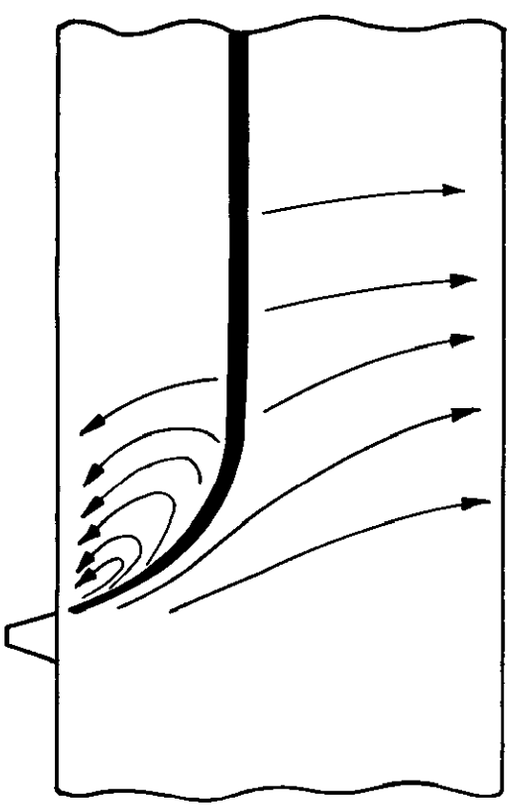

(f) ROUND LEADING EDGE WITH ISOLATED STRAKE
($\alpha = 8 \cdot 1°$)

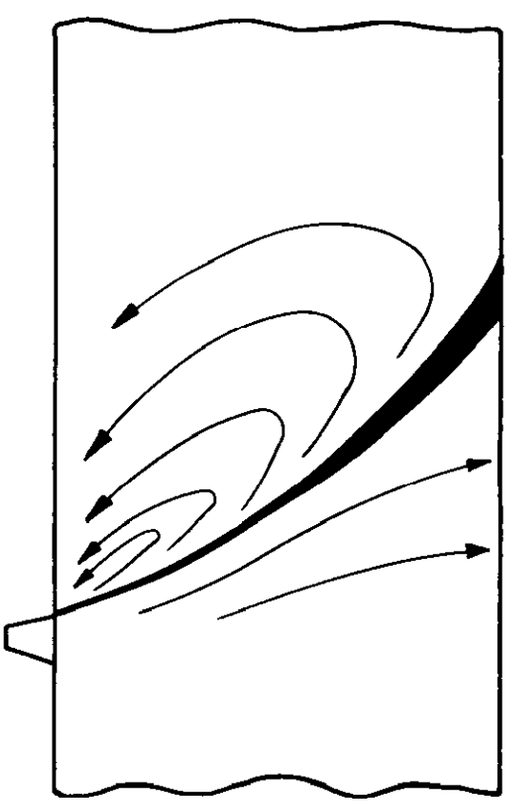

(f) ROUND LEADING EDGE WITH ISOLATED STRAKE
($\alpha = 12 \cdot 1°$)

FIG. 11. SURFACE FLOW DIAGRAMS.

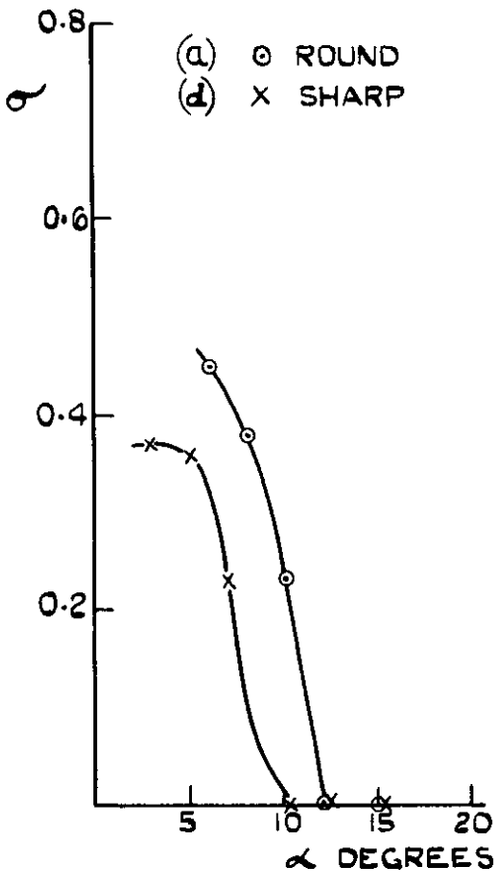

(a) ROUND AND (d) SHARP LEADING EDGES

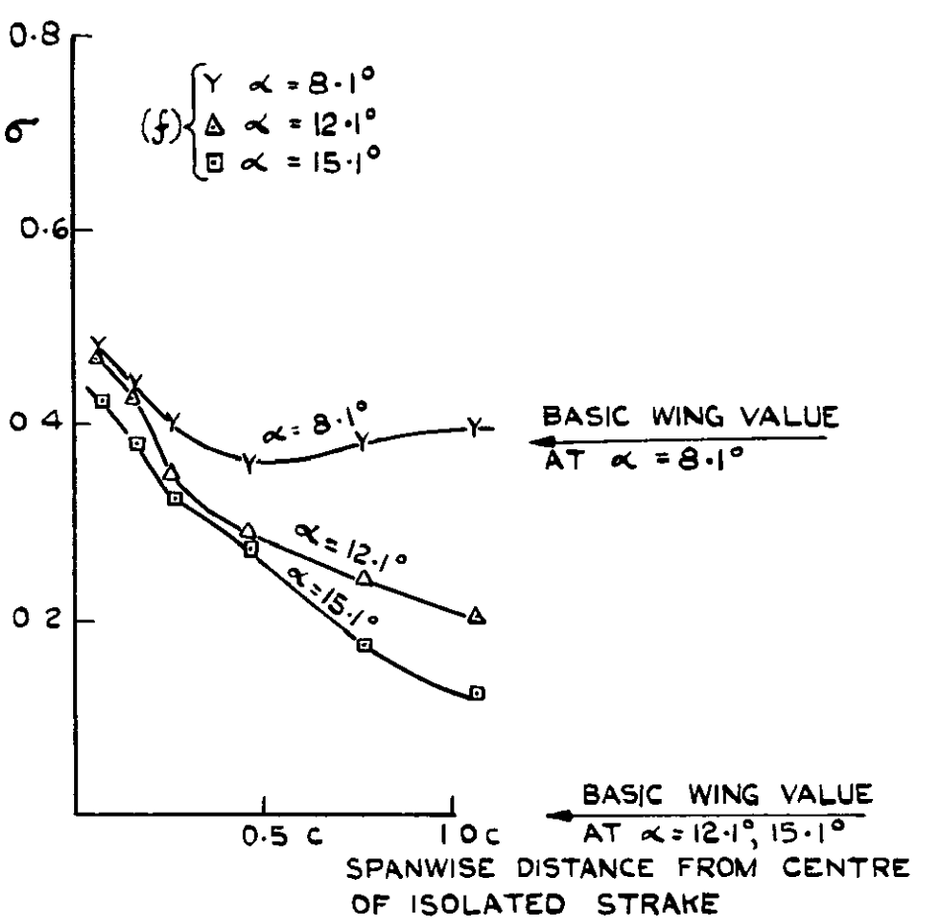

(f) ROUND LEADING EDGE WITH ISOLATED STRAKE

FIG.12. VARIATIONS OF UPPER SURFACE RECOVERY FACTOR.

$$\sigma = \frac{C_{P2} - C_{P1}}{1 - C_{P1}}$$

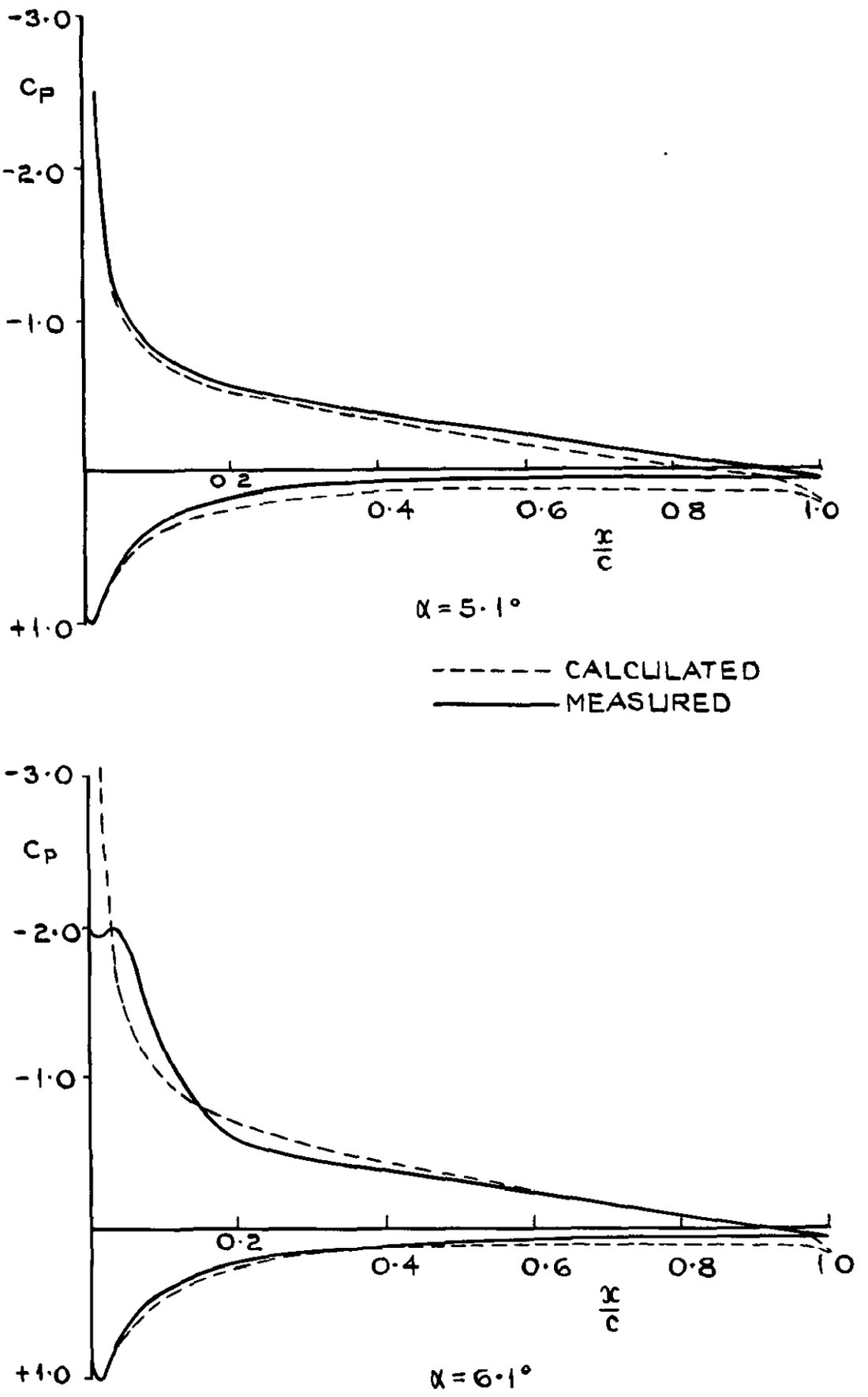

FIG.13. COMPARISON BETWEEN CALCULATED & MEASURED PRESSURE DISTRIBUTIONS FOR (a) ROUND LEADING EDGE.

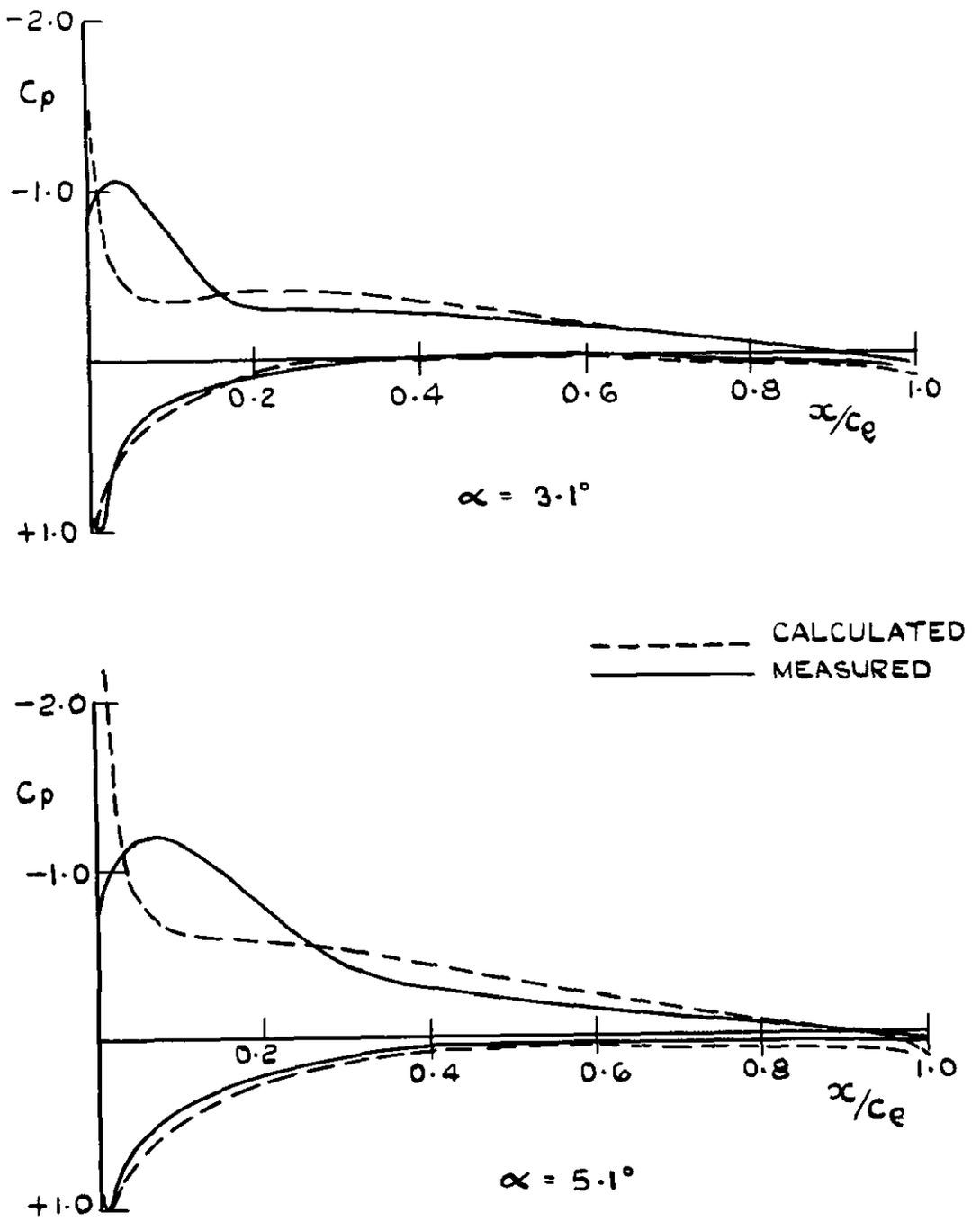

FIG. 14. COMPARISON BETWEEN CALCULATED AND MEASURED PRESSURE DISTRIBUTIONS FOR (d) SHARP LEADING EDGE.

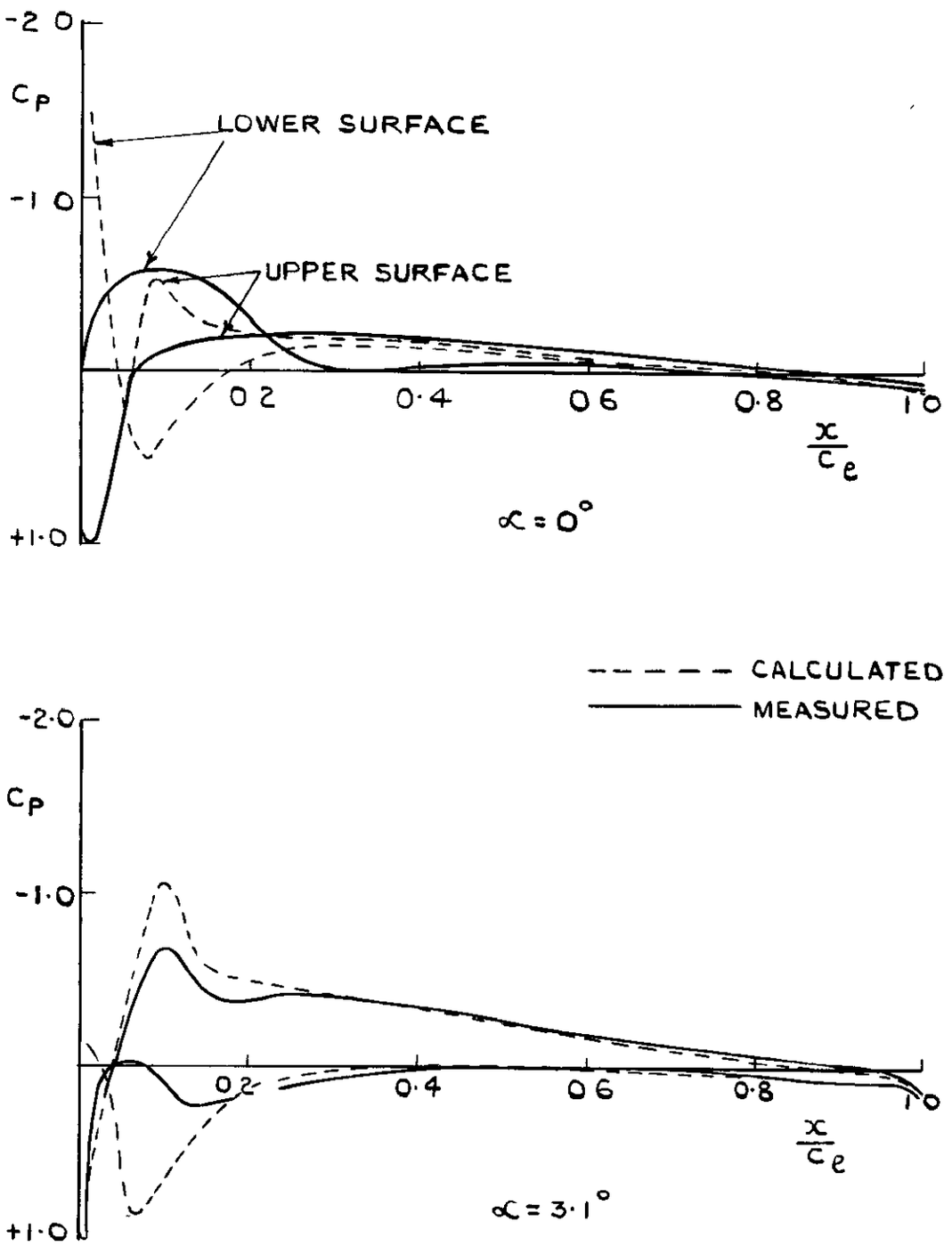

FIG. 15. COMPARISON BETWEEN CALCULATED & MEASURED PRESSURE DISTRIBUTIONS FOR (e) SHARP LEADING EDGE - NOSE FLAP DEFLECTED 25°.

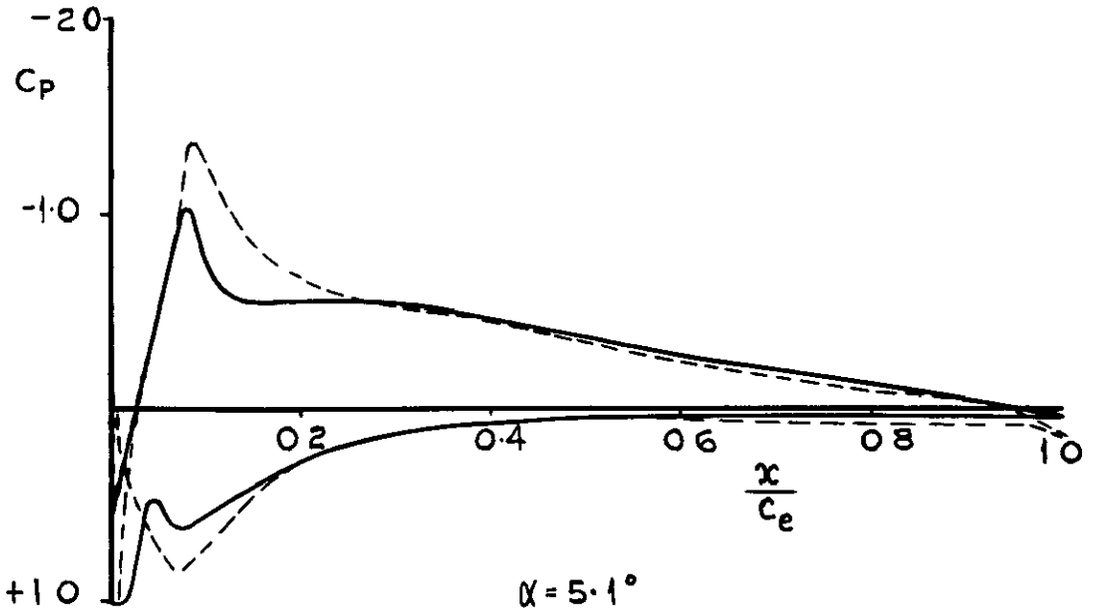
-2·0
C_P
-1·0
+1·0
0·2
0·4
0·6
0·8
1·0
$\frac{x}{c_e}$
α = 5·1°

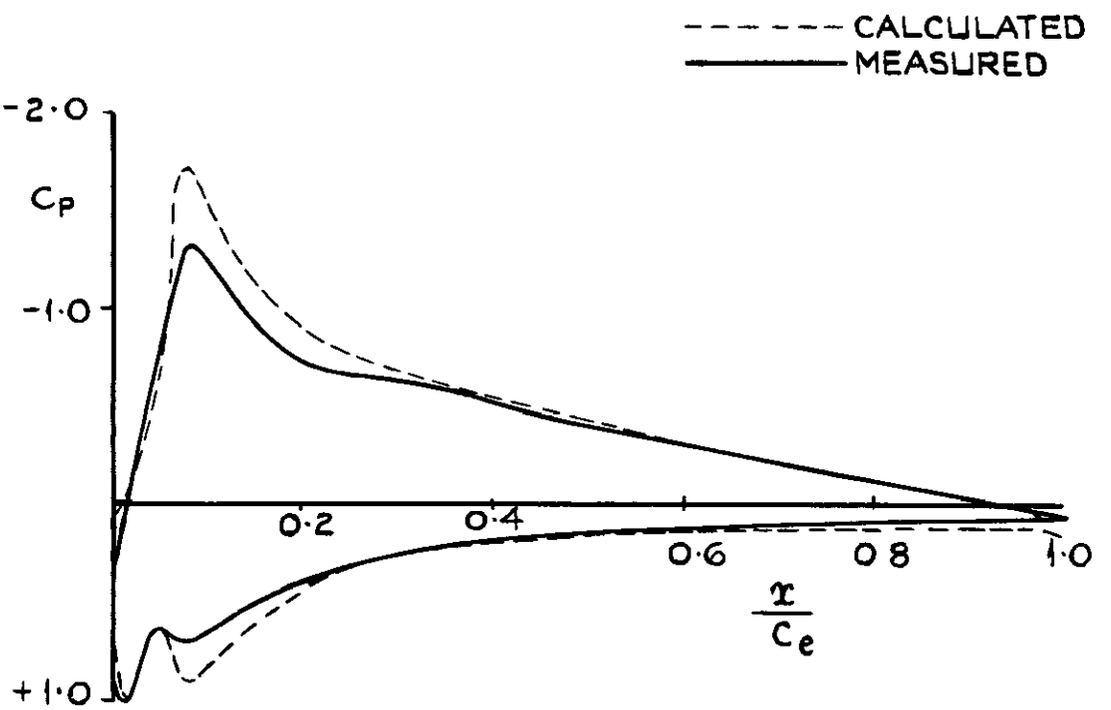
CALCULATED
MEASURED
-2·0
C_P
-1·0
+1·0
0·2
0·4
0·6
0·8
1·0
$\frac{x}{c_e}$
α = 7·1°

FIG. 15. (Cont)

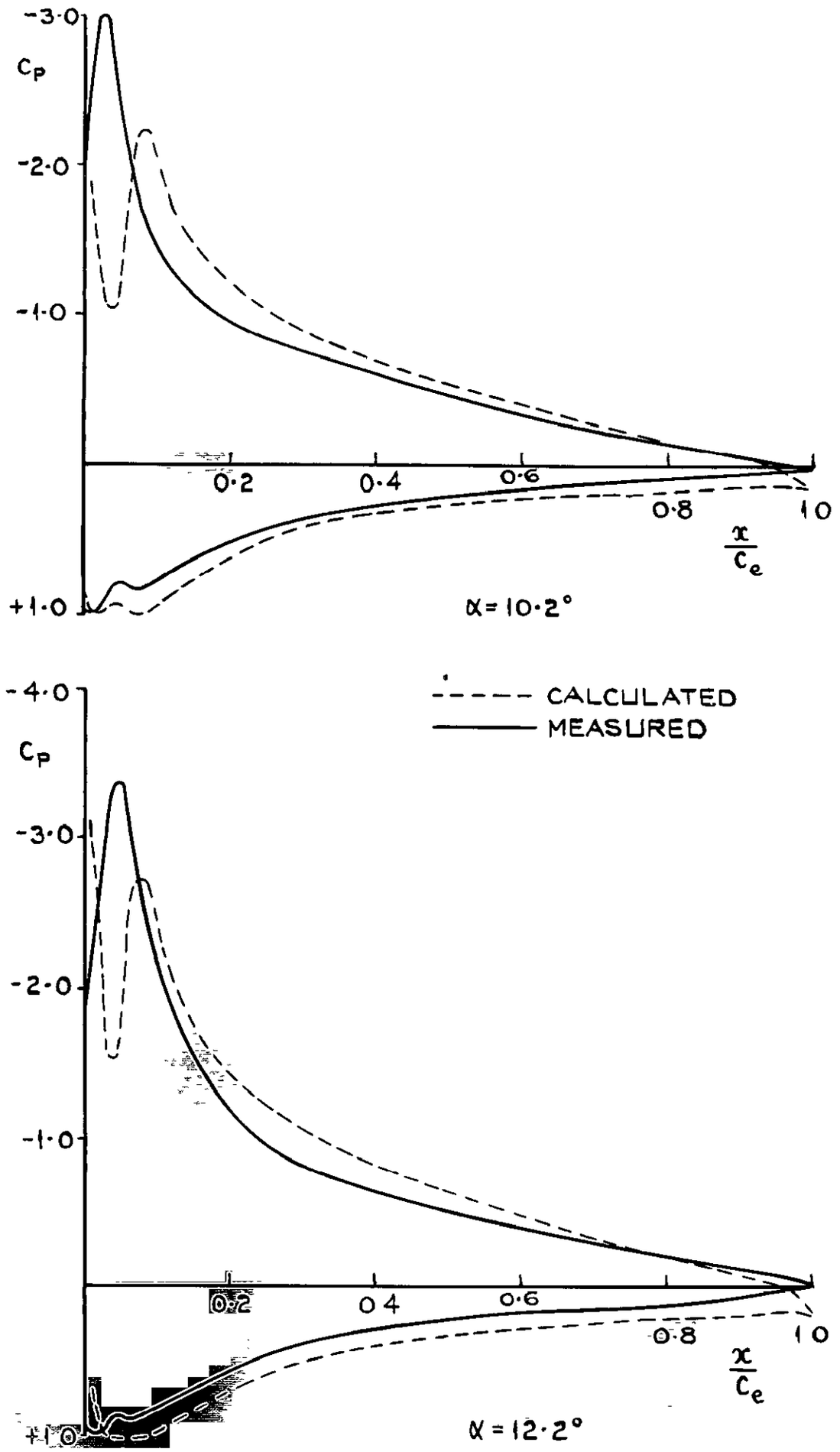
-3·0
C_p
-2·0
-1·0
+1·0
0·2
0·4
0·6
0·8
1·0
$\frac{x}{c_e}$
α = 10·2°
CALCULATED
MEASURED
-4·0
C_p
-3·0
-2·0
-1·0
+1·0
0·2
0·4
0·6
0·8
1·0
$\frac{x}{c_e}$
α = 12·2°

FIG. 15. (Cont)

C.P. No. 410
(20,397)
A.R.C. Technical Report

Published by
HER MAJESTY'S STATIONERY OFFICE

To be purchased from
York House, Kingsway, London W C 2
423 Oxford Street, London W 1
13A Castle Street, Edinburgh 2
109 St. Mary Street, Cardiff
39 King Street, Manchester 2
Tower Lane, Bristol 1
2 Edmund Street, Birmingham 3
80 Chichester Street, Belfast
or through any bookseller

Printed in Great Britain

S.O. Code No. 23-9011-10

C.P. No. 410